Journal of Theoretical Biology 256 (2009) 14–28

Contents lists available at ScienceDirect

Journal of Theoretical Biology

journal homepage: www.elsevier.com/locate/yjtbi

# The diffusive influx and carrier efflux have a strong effect on the bistability of the *lac* operon in *Escherichia coli*

Jason T. Noel [a], Sergei S. Pilyugin [b], Atul Narang [c,*]

[a] Department of Chemical Engineering, University of Florida, Gainesville, FL 32611-6005, USA
[b] Department of Mathematics, University of Florida, Gainesville, FL 32611-8105, USA
[c] Center for Applied Mathematics, University of Florida, Gainesville, FL 32611-8105, USA

ARTICLE INFO

*Article history:*
Received 1 February 2008
Received in revised form
2 September 2008
Accepted 4 September 2008
Available online 18 September 2008

*Keywords:*
Mathematical model
Induction
Lactose operon
Hysteresis

ABSTRACT

In the presence of gratuitous inducers, the *lac* operon of *Escherichia coli* exhibits bistability. Most models in the literature assume that the inducer enters the cell via the carrier (permease), and exits by a diffusion-like process. The diffusive influx and carrier efflux are neglected. However, analysis of the data shows that in non-induced cells, the diffusive influx is comparable to the carrier influx, and in induced cells, the carrier efflux is comparable to the diffusive efflux. Since bistability entails the coexistence of steady states corresponding to both non-induced and induced cells, neither one of these fluxes can be ignored. We present a model accounting for both fluxes, and show that: (1) The thresholds (i.e., the extracellular inducer levels at which transcription turns on or off) are profoundly affected by both fluxes. The diffusive influx reduces the on threshold, and eliminates irreversible bistability, a phenomenon that is inconsistent with data. The carrier efflux increases the off threshold, and abolishes bistability at large permease activities, a conclusion that can be tested experimentally. (2) The thresholds are well approximated by simple analytical expressions obtained by considering two limiting cases (no carrier efflux and no diffusive influx). (3) The simulations are in good agreement with the data for isopropyl thiogalactoside (IPTG), but somewhat discrepant with respect to the data for thiomethyl galactoside (TMG). We discuss the potential sources of the discrepancy.



## 1. Introduction

Many of the early studies of the *lac* operon were concerned with the kinetics of enzyme induction in the presence of *gratuitous* inducers, such as thiomethyl galactoside (TMG) and isopropyl thiogalactoside (IPTG), which cannot be hydrolyzed by $\beta$-galactosidase. It turns out that lactose, the natural inducer of the *lac* operon, stimulates not only the synthesis of the lactose enzymes, but also their dilution by growth. Gratuitous inducers were used because they allowed the kinetics of enzyme synthesis to be separated from the masking effect of dilution. This was achieved by growing the cells in a medium containing a gratuitous inducer (which promotes lactose enzyme synthesis, but not growth), and non-galactosidic carbon sources, such as succinate, glycerol, or glucose (which support growth, but not lactose enzyme synthesis).

These early studies showed that enzyme synthesis was bistable: Pre-induced cells remained induced, and non-induced cells remained non-induced (Cohn and Horibata, 1959; Novick and Weiner, 1957). Furthermore, bistability disappeared in (cryptic) mutants lacking permease. It was proposed that bistability occurred due to the destabilizing effect of the positive feedback generated by *lac* permease: The permease catalyzes accumulation of the inducer, which in turn stimulates the synthesis of even more permease.

Recently, Ozbudak et al. (2004) performed detailed studies of *lac* bistability during growth of *Escherichia coli* K12 MG1655 on TMG and succinate/glucose. To this end, they inserted two reporter operons into the bacterial chromosome:

- The reporter *lac* operon, placed under the control of the *lac* promoter, coded for green fluorescent protein (GFP) instead of the *lac* enzymes. Thus, the GFP intensity of a cell provided a measure of the *lac* enzyme level.
- The reporter *gat* operon, placed under the control of the constitutive *gat* promoter, coded for the red fluorescent protein (RFP) instead of the *gat* enzymes. The RFP intensity of a cell provided a measure of its CRP–cAMP level.

They observed that when the cells were grown in the presence of succinate and various concentrations of TMG, they exhibited

* Corresponding author.
*E-mail address:* narang@che.ufl.edu (A. Narang).

0022-5193/$ - see front matter © 2008 Elsevier Ltd. All rights reserved.
doi:10.1016/j.jtbi.2008.09.003

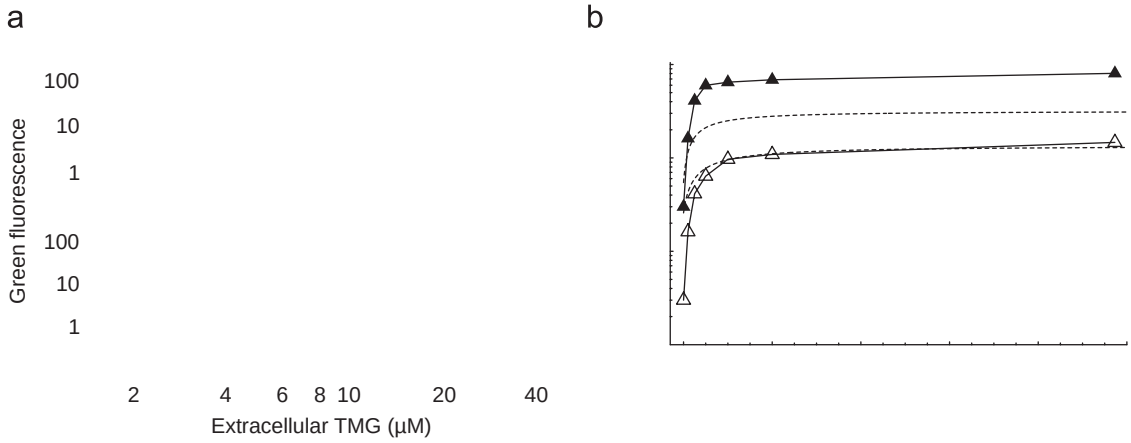


**Fig. 1.** Bistability of the *lac* operon during growth of *E. coli* K12 MG1655 on succinate and succinate + glucose (Ozbudak et al., 2004, Figs. 2b and c). (a) Bistability during growth on succinate and various concentrations of extracellular TMG. The (normalized) green fluorescence provides a measure of the steady state activity of the *lac* operon. The upper (resp., lower) panel shows the green fluorescence observed during exponential growth of induced (resp., non-induced) cells on a mixture of succinate and various concentrations of extracellular TMG. Bistability occurs at extracellular TMG concentrations between the off and on thresholds at 3 and 30 mM, respectively. (b) Bistability persists even if glucose is added to the mixture of succinate and TMG. The lower (n ) and upper (m) curves show the off and on thresholds observed at various glucose concentrations. The dashed curves show the thresholds predicted by our model with the parameter values in Table 1.

bistability (Fig. 1a). Moreover, the bistability persisted even if glucose was added to the mixture of succinate and TMG, but the thresholds increased with the concentration of extracellular glucose (Fig. 1b). Both observations were mirrored by the bifurcation diagram for the equations

$$\frac{dx}{dt} = r_s - r_x - r_g x; \quad r_s \equiv V_s(G) e \frac{s}{K_1 + s}; \quad r_x \equiv k_x x, \tag{1}$$

$$\frac{de}{dt} = r_e^+ - r_e^- - r_g e; \quad r_e^+ \equiv V_e(G) \frac{1 + K_x^2 x^2}{1 + \alpha + K_x^2 x^2}; \quad r_e^- \equiv k_e^- e, \tag{2}$$

where $x; e$ denote the intracellular TMG and *lac* permease levels, respectively, $s; G$ denote the extracellular TMG and glucose levels, respectively, $r_s; r_x$ denote the rates of carrier influx and diffusive efflux, respectively, $V_s(G); V_e(G)$ are decreasing functions of $G$ accounting for the inhibitory effects of glucose on inducer uptake (inducer exclusion) and *lac* expression (cAMP-CRP mediated repression), respectively, $r_g$ denotes the specific growth rate on succinate/glucose, and $r_e^+; r_e^-$ denote the rates of permease synthesis and degradation, respectively.

To quantify the variation of $V_e$ with $G$, they measured the average green and red fluorescence intensities of cells growing exponentially in a medium containing a high concentration of TMG, a fixed concentration of succinate, and various concentrations of glucose. They found that the green and red fluorescence intensities, scaled by the corresponding values observed in a medium containing no glucose, were equal at all glucose concentrations (Ozbudak et al., 2004, Fig. 3b). Moreover, the scaled RFP intensity decreased 5-fold at saturating glucose concentrations (Fig. 2). It was concluded that in the presence of 1 mM glucose, $V_e$ decreases 5-fold due to cAMP-CRP mediated repression. This is somewhat higher than the maximum possible cAMP-mediated repression in *E. coli* K12 MG1655. Recently, Kuhlman et al., found that during growth of this strain on 0.5% glucose and 1 mM IPTG, variation of the extracellular cAMP level from 0 to 10 mM produces no more than a 3-fold change in *lac* expression (Kuhlman et al., 2007, Fig. 1B).

One of the goals of this work is to resolve the foregoing discrepancy between the data obtained by Ozbudak et al. and Kuhlman et al. More importantly, we wish to extend the above model in three ways.

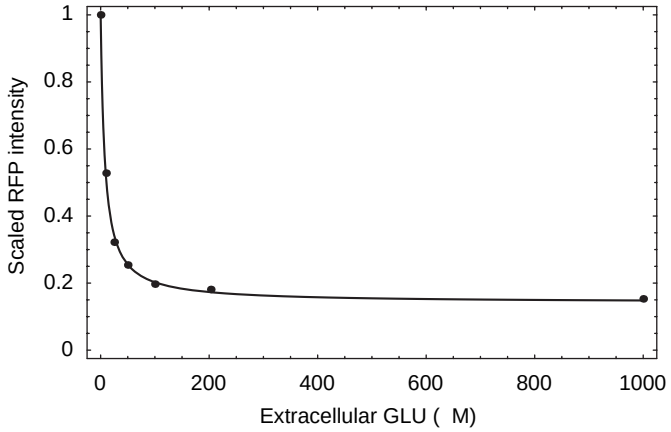


**Fig. 2.** During exponential growth of *E. coli* K12 MG1655 on succinate, TMG, and various concentrations of glucose, the red fluorescence intensity decreases with the concentration of glucose (Ozbudak et al., 2004, Fig. 3a). The curve shows the fit to Eq. (28).

*Induction kinetics*: The above expression for the *lac* induction rate, $r_e^+$, is based on a molecular model that is inconsistent with the data. Specifically, it assumes that the *lac* operon contains one operator, the *lac* repressor contains two inducer-binding sites, and *lac* repression is entirely due to repressor–operator binding (Yagil and Yagil, 1971). However, the data shows that the *lac* operon contains two auxiliary operators, $O_2$ and $O_3$ (in addition to the main operator, $O_1$); the *lac* repressor is a tetramer containing four inducer-binding sites (Lewis, 2005); and more than 95% of the repression is due to the formation of DNA loops rather than repressor-operator binding (Oehler et al., 1990, 1994).

A kinetic model taking due account of the three operators and four inducer-binding sites yields

$$r_e^+ \equiv V_e \frac{1}{1 + \alpha=(1 + K_x x)^2 + \hat{\alpha}=(1 + K_x x)^4}, \tag{3}$$

where $K_x$ is the association constant for repressor-inducer binding, and $\alpha; \hat{\alpha}$ are related to the repression stemming from repressor–operator binding and DNA looping, respectively

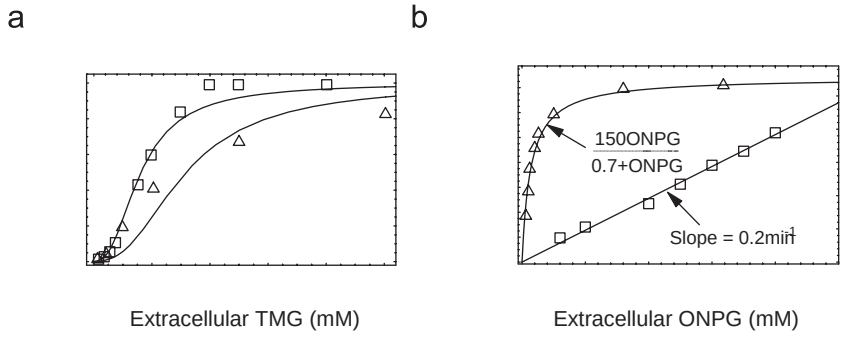


**Fig. 3.** The kinetics of induction and diffusive influx (Herzenberg, 1959, Figs. 1 and 4). (a) Variation of the scaled induction rate with extracellular TMG and IPTG levels (measured with the cryptic mutant, *E. coli* ML3). The full curves show the fits to the data obtained with Eq. (3) and the parameter values $\alpha = 40$, $\hat{x} = 1200$, $K_x^{-1} = 24$ mM for IPTG, and $K_x^{-1} = 470$ mM for TMG. (b) Variation of the ONPG hydrolysis rate with the extracellular ONPG concentration in cryptic (*lacY*$^-$) mutants and fully induced wild-type (WT) cells of *E. coli* ML30. The rates were converted from mmol min$^{-1}$ mgdw$^{-1}$ to mM min$^{-1}$ by assuming that there are 2.7 mL of cell water per gdw (Winkler and Wilson, 1966).

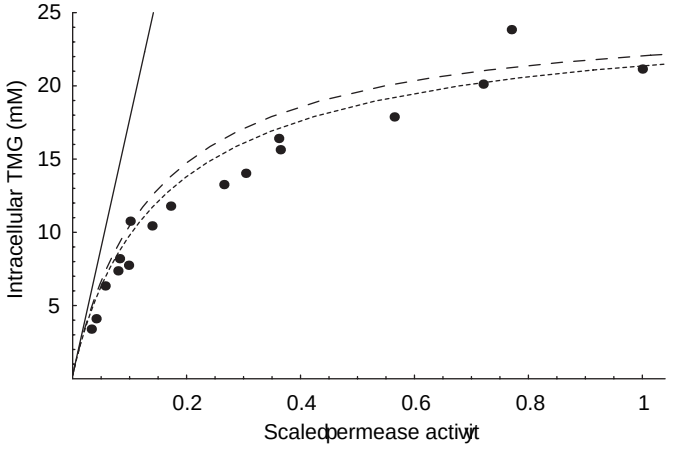


**Fig. 4.** Existence and quantification of the carrier efflux (Maloney and Wilson, 1973). When *E. coli* K12 CA8000, induced to various levels, is exposed to chloramphenicol and 0.24 M extracellular TMG, the steady state intracellular TMG level (•) increases hyperbolically with the scaled permease activity (normalized by the activity of fully induced cells). The short- and long-dashed curves show the intracellular TMG levels predicted by Eqs. (4) and (21), respectively, which are based on models accounting for the carrier efflux. The full line shows the intracellular TMG level predicted by Eq. (4) in the absence of the carrier efflux.

(Narang, 2007). Kinetic analysis shows that the expression for $r_e^+$ shown in Eq. (2) cannot fit the data obtained at low inducer concentrations (Narang, 2007, Figs. 10a and 14). In contrast, (3) yields good fits to the entire induction curve obtained with various gratuitous inducers (Fig. 3a) and wild-type or mutant strains (Narang, 2007, Figs. 5, 11 and A.1).

Eq. (3) is based on the following assumptions: (1) The repressor dimer binds to an operator only if it is inducer-free. (2) Binding of the repressor to $O_1$ or $O_3$ blocks transcription completely, whereas binding to $O_2$ has no effect. (3) The affinity of the repressor for $O_2$ or $O_3$ is small compared to its affinity for $O_1$. (4) All four inducer-binding sites of the repressor are identical and independent. Based on similar assumptions, Kuhlman et al. arrived at the very same expression by using the statistical thermodynamic, rather than kinetic, approach (Kuhlman et al., 2007). Recently, a more complex expression containing 76 terms has been obtained by relaxing the first two assumptions (Saiz and Vilar, 2008). Specifically, it is assumed that (a) even inducer-bound dimers bind to the repressor, but with a relatively small affinity, and (b) the binding of the repressor to $O_3$ reduces the transcription rate by 97% (rather than 100%).

*Diffusive influx*: It is well known that in addition to the carrier influx, there is a diffusive influx. Fig. 3b shows that even cryptic cells hydrolyze ONPG, and the hydrolysis rate increases linearly with the extracellular ONPG concentration.[1] It follows that gratuitous inducers can enter the cells by a permease-independent mechanism, and the influx rate can be formally described by the first-order kinetics, $k_x s$. The data also implies that over the range of sugar concentrations used in the experiments (t 1 mM), the diffusive influx is ~0:1% of the carrier influx in fully induced cells. However, in non-induced cells, which contain only ~0:1% of the permease in induced cells (Maloney and Wilson, 1973), the diffusive influx must be comparable to the carrier influx.

*Carrier efflux*: The existence of the carrier efflux was suggested in early studies with gratuitous inducers (Koch, 1964). However, Maloney and Wilson (1973) were the first to quantify its effect. To this end, they measured the steady state intracellular TMG levels in cells that were induced to various levels, and then exposed to chloramphenicol plus 0.24 mM extracellular TMG (Fig. 4). The data obtained cannot be reconciled with models that do not account for the carrier efflux. Indeed, since enzyme synthesis is blocked in the presence of chloramphenicol, and the dilution rate of the inducer, $r_g x$, is negligibly small, these models imply that $x$ increases linearly with the scaled enzyme activity (full line in Fig. 4), whereas experiments show that $x$ increases hyperbolically (closed circles in Fig. 4).

To resolve the above discrepancy, Maloney and Wilson proposed that the permease supports influx and efflux, and the efflux rate is $V_s ex=(K_2 + x)$. The steady state intracellular TMG level therefore satisfies the equation

$$0 = \frac{dx}{dt} = (V_s e_*) \quad \frac{s}{K_1 + s} - \frac{x}{K_2 + x} \quad - k_x(x - s); \qquad \equiv \frac{e}{e_*}, \tag{4}$$

where $e_*$ is the activity of the fully induced cells. They measured $k_x$ (0:14 min$^{-1}$), $V_s e_*$ (106 mmol min$^{-1}$ mL$^{-1}$), $s$ (0.24 mM), $K_1$ (0.8 mM), and showed that if $K_2$ is chosen to be 84 mM, Eq. (4) yields a good fit to the data (short-dashed curve in Fig. 4). This modified model implies that in induced cells, 80% of the efflux is due to the carrier (Maloney and Wilson, 1973, Fig. 6).

It is therefore clear that the carrier efflux cannot be ignored in induced cells, and the diffusive influx cannot be neglected in non-induced cells. Since bistability entails the coexistence of steady states corresponding to both induced and non-induced cells, neither the carrier efflux nor the diffusive influx can be neglected.

[1] ONPG diffuses into the cell roughly twice as fast as TMG: In *lacY*$^-$ strains of *E. coli* ML30, the rate constants for diffusion of ONPG and TMG are 0:2 min$^{-1}$ (Fig. 3b) and 0:14 min$^{-1}$ (Section 2), respectively. The carrier influx of ONPG is also ~2 times the carrier influx of TMG (Maloney and Wilson, 1973, Fig. 1).

Yet, most models in literature have ignored one of the fluxes (Chung and Stephanopoulos, 1996; Tian and Burrage, 2005), or both of them (Babloyantz and Sanglier, 1972; van Hoek and Hogeweg, 2006; Narang and Pilyugin, 2008; Ozbudak et al., 2004; Santillán et al., 2007; Savageau, 2001). Only one study accounted for both fluxes (Vilar et al., 2003), but the effect of the fluxes on bistability was not analyzed. The goal of this work is to analyze this effect.

Recently, we studied the effect of DNA looping on the bistability of *lac* operon (Narang and Pilyugin, 2008, Sections 3.1.1–3.1.2). It was shown therein that the steady states are qualitatively and quantitatively different in the presence of DNA looping. In particular, the bistable region is significantly larger if the repression is primarily due to DNA looping. Here, we formulate and analyze an extended model that accounts for DNA looping as well as the diffusive influx and the carrier efflux. We find that:

(1) The diffusive influx has no effect on the off threshold, but it significantly reduces the on threshold. It also changes the nature of the bistability. In the absence of the diffusive influx, bistability is irreversible, a result that is inconsistent with the data. This inconsistency disappears in the presence of the diffusive influx.
(2) The carrier efflux has no effect on the on threshold, but it significantly increases the off threshold. Moreover, its existence implies that there can be no bistability in cells overexpressing the permease.
(3) The variation of the on and off thresholds with the extracellular glucose concentration can be captured by simple analytical expressions.

The extended model yields good agreement with the bistability data for IPTG, but there is a discrepancy with respect to the data for TMG. We discuss the potential sources of this discrepancy.

## 2. Model

Fig. 5 shows the kinetic scheme of the model. We assume that:

(1) The concentrations of the permease, intracellular inducer, GFP, and RFP, denoted $e$, $x$, $g$, and $r$, respectively, are based on the total volume of the cells (mol $L^{-1}$). The concentrations of the extracellular inducer and glucose, denoted $s$ and $G$, respectively, are based on the volume of the culture (mol $L^{-1}$). The rates of all the processes are based on the total volume of the cells (mol $h^{-1}$ $L^{-1}$).

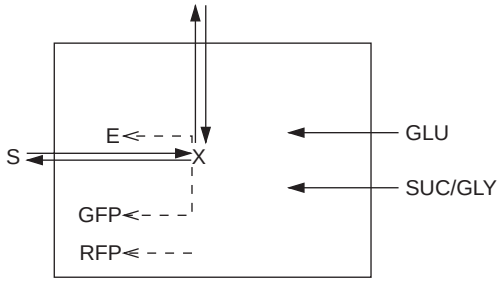


**Fig. 5.** Kinetic scheme of the model. Here, $E$ denotes *lac* permease; $S$ and $X$ denote the extracellular and intracellular inducer, respectively; GFP and RFP denote the green and red fluorescent protein synthesized by the reporter *lac* and constitutive *gat* operons, respectively; and GLU, SUC, GLY denote glucose, succinate, and glycerol.

The choice of these units implies that if the concentration of any intracellular component, $Z$, is $z$ mol $L^{-1}$, then the evolution of $z$ is given by

$$\frac{dz}{dt} = r_z^+ - r_z^- - r_g z,$$

where $r_z^+$ and $r_z^-$ denote the rates of synthesis and degradation of $Z$ in mol $h^{-1}$ $L^{-1}$, and $r_g$ is the specific growth rate in $h^{-1}$.

(2) The specific growth rate is given by

$$r_g \equiv \phi_g(G) r_{g0},$$

where $r_{g0}$ is the specific growth rate in the absence of glucose (i.e., in the presence of pure succinate), and $\phi_g(G)$ is an increasing function of $G$ such that $\phi_g(0) = 1$, which accounts for the increase of the specific growth rate produced by addition of glucose to a culture growing on succinate.

(3) The net carrier-mediated uptake rate of $S$ is

$$r_s \equiv \phi_s(G) V_{s0} e \frac{s/K_1 - x/K_2}{1 + s/K_1}, \tag{5}$$

where $\phi_s(G)$ is a decreasing function of $G$ such that $\phi_s(0) = 1$, which accounts for the inhibition of inducer uptake due to inducer exclusion.

Eq. (5) is based on Kaback's *alternating access* model for permease-mediated transport (Fig. 6a). This model yields the expression

$$r_s = \phi_s(G) e \frac{a_1 s - a_2 x}{a_3 + a_4 s + a_5 x + a_6 s x}, \tag{6}$$

where $a_i$; $i = 1;6$ are functions of the rate constants, $k_i^+$; $k_i^-$; $i = 1;4$, shown in Fig. 6a (Segel, 1975, Chapter IX). However, the data shows that over the range of galactoside concentrations typically used in the experiments (0p $st$ 1 mM), the carrier-mediated influx rate is essentially independent of $x$: The initial uptake rate does not change even if the cells are preloaded with intracellular galactoside (Fig. 6b). It follows that under typical experimental conditions, the terms, $a_5 x$ and $a_6 s x$, are negligible.[2] Thus, (6) reduces to (5) with $V_s = a_1/a_4$, $K_1 = a_3/a_4$, and $K_2 = a_1 a_3/(a_2 a_4)$. Eq. (5) implies that the initial efflux rate is proportional to $x$. This is consistent with the data in several studies (Kepes, 1969; Koch, 1964; Lancaster et al., 1975).

(4) The net rate of expulsion of $X$ by diffusion follows the kinetics

$$r_x \equiv k_x (x - s).$$

We assume that $k_x = 0{:}14\,\mathrm{min}^{-1}$. This is the value obtained by Maloney and Wilson. We found that this value also provides a good fit to the data for TMG uptake in the *lacY*$^-$ strain *E. coli* ML3 (Kepes, 1960, Fig. 9).

(5) The intracellular inducer stimulates the transcription of the native and reporter *lac* operons, resulting in the synthesis of the *lac* enzymes and GFP, respectively.

(a) The synthesis rate of the permease, $E$, is

$$r_e \equiv \phi_{e;lac}(G) V_{e0} \frac{1}{1 + \alpha/(1 + K_x x)^2 + \beta/(1 + K_x x)^4}, \tag{7}$$

where $V_{e0}$ is the synthesis rate in fully induced cells growing on succinate ($G = 0$), $\phi_{e;lac}(G)$ is a decreasing function of $G$ satisfying $\phi_{e;lac}(0) = 1$, which accounts for the repression of *lac* expression due to reduction of CRP–cAMP levels in the presence of glucose, $K_x$ is the

[2] This is probably due to the low value of $k_3^-$, the rate constant for binding of intracellular sugar to the permease, since $a_5; a_6$ are proportional to $k_3^-$, whereas $a_3; a_4$ are independent of $k_3^-$ (Segel, 1975, Eq. (IX-45)).

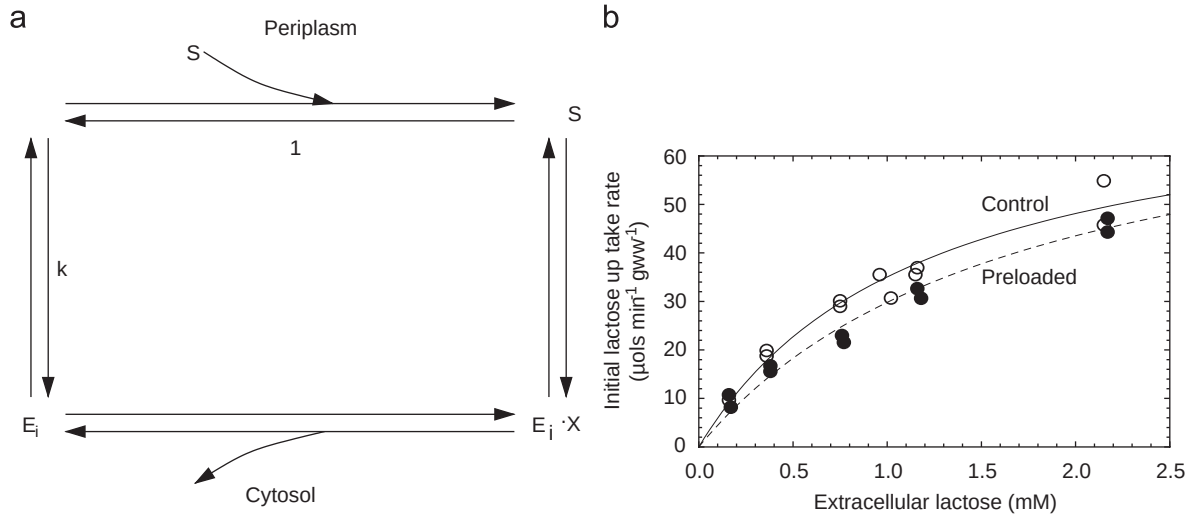


**Fig. 6.** Kinetics of permease-mediated transport. (a) The simplified alternating access model obtained by neglecting the protonation and deprotonation steps (adapted from Fig. 6 of Abramson et al., 2003). Here, $E_o$ denotes the outward-facing conformation of the permease, which binds the periplasmic sugar, $S$, to form $E_o \cdot S$. This complex undergoes a conformational change to produce $E_i \cdot X$, which dissociates, thus liberating the intracellular sugar, $X$, and the inward-facing conformation, $E_i$. The latter reverts to $E_o$ by a conformational change. (b) The initial lactose uptake rates observed in control cells ($x \approx 0$) and preloaded cells ($x4$ 0) of the *lacZ*$^-$ constitutive mutant, *E. coli* ML308-225, are virtually identical at all extracellular lactose concentrations up to 2 mM (Winkler and Wilson, 1966, Fig. 12). Similar results are obtained with ONPG (Winkler and Wilson, 1966, Fig. 11) and TMG (Kepes, 1960, Fig. 1).

association constant for repressor-inducer binding, and $\alpha$; $\hat{\alpha}$ characterize the repression due to repressor–operator binding and DNA looping, respectively.

The values of $\alpha$ and $\hat{\alpha}$ are 20–50 and ~1200, respectively, which reflect the fact that more than 95% of the total repression, $1+\alpha+\hat{\alpha}$, is due to the formation of DNA loops (Oehler, 1990, 1994). The dissociation constant for repressor-inducer binding, $K_x^{-1}$, is 72 30 mM for IPTG (Narang, 2007, Table 1). It is 10 times higher for TMG, based on a simple analysis of the data with Scatchard plots (Barkley et al., 1975, Table 1). Similar estimates are obtained when Eq. (3) is used to fit the data in Fig. 3a. Assuming $\alpha = 40$ and $\hat{\alpha} = 1200$, the best fits are obtained when the dissociation constants for IPTG and TMG are 24 and 470 mM, respectively.

(b) The synthesis rate of GFP is

$$r_{GFP} \equiv V_{e0}\phi_{e;lac}(G)\frac{1}{1+\alpha=(1+K_x x)^2+\hat{\alpha}_G=(1+K_x x)^4},$$

where $\hat{\alpha}_G$o $\hat{\alpha}$. This expression is obtained by assuming that the promoters of the reporter and native *lac* operons are identical, so that both operons have the same maximum synthesis rates in the absence of glucose, and are subject to the very regulation by CRP–cAMP and repressor–operator binding. However, the two operons differ with respect to regulation by DNA looping because the reporter *lac* operon lacks the auxiliary operator, $O_2$, which precludes the formation of DNA loops by interaction between $O_1$ and $O_2$.

Ozbudak et al. (2004) estimated the total repression of the *lac* reporter, $1+\alpha+\hat{\alpha}_G$, to be 170, which implies that $\hat{\alpha}_G \approx 130$.

(6) The synthesis rate of RFP follows the constitutive kinetics

$$r_{RFP} \equiv \phi_{e;gat}(G)V_{r0},$$

where $V_{r0}$ is the synthesis rate of RFP in the absence of glucose and $\phi_{e;gat}(G)$ is a decreasing function of $G$ such that $\phi_{e;gat}(0) = 1$, which accounts for the CRP–cAMP effect exerted in the presence of glucose.

(7) Degradation of *lac* enzymes and GFP is negligible.

Given these assumptions, the mass balances yield

$$\frac{dx}{dt} = \phi_s V_{s0} e \frac{s=K_1 - x=K_2}{1+s=K_1} - k_x(x-s) - \phi_g r_{g0} x, \tag{8}$$

$$\frac{de}{dt} = \phi_{e;lac} V_{e0} \frac{1}{1+\alpha=(1+K_x x)^2+\hat{\alpha}=(1+K_x x)^4} - \phi_g r_{g0} e, \tag{9}$$

$$\frac{dg}{dt} = \phi_{e;lac} V_{e0} \frac{1}{1+\alpha=(1+K_x x)^2+\hat{\alpha}_G=(1+K_x x)^4} - \phi_g r_{g0} g, \tag{10}$$

$$\frac{dr}{dt} = \phi_{e;gat} V_{r0} - r_{g0}\phi_g r. \tag{11}$$

Ozbudak et al. scaled the GFP and RFP intensities by the corresponding intensities observed during steady exponential growth on succinate and excess TMG, but no glucose. Under these conditions, Eqs. (9)–(11) imply that $e$, $g$, and $r$ have the values $e_* \equiv V_{e0}=r_{g0}$, $g_* \equiv V_{e0}=r_{g0}$, and $r_* \equiv V_{r0}=r_{g0}$, respectively. Thus, we are led to define the dimensionless variables

$$\equiv \frac{e}{e_*}; \quad \gamma \equiv \frac{g}{g_*}; \quad \rho \equiv \frac{r}{r_*}.$$

If we scale the remaining variables, $x$ and $t$, as follows:

$$\chi \equiv \frac{x}{K_x^{-1}}; \quad \tau \equiv \frac{t}{r_{g0}^{-1}},$$

we arrive at the dimensionless equations

$$\tau_x \frac{d\chi}{d\tau} = \phi_s \delta_{m0} \frac{\sigma=\kappa_1 - \chi=\kappa_2}{1+\sigma=\kappa_1} - (\chi-\sigma) - \tau_x \phi_g \chi, \tag{12}$$

$$\frac{d}{d\tau} = \phi_{e;lac} f(\chi) - \phi_g \; ; \quad f(\chi) \equiv \frac{1}{1+\alpha=(1+\chi)^2+\hat{\alpha}=(1+\chi)^4}, \tag{13}$$

$$\frac{d\gamma}{d\tau} = \phi_{e;lac} h(\chi) - \phi_g \gamma; \quad h(\chi) \equiv \frac{1}{1+\alpha=(1+\chi)^2+\hat{\alpha}_G=(1+\chi)^4}, \tag{14}$$

$$\frac{d\rho}{d\tau} = \phi_{e;gat} - \phi_g \rho, \tag{15}$$

with the dimensionless parameters,

$$\sigma \equiv \frac{s}{K_x^{-1}}; \quad \kappa_i \equiv \frac{K_i}{K_x^{-1}}; \quad \tau_x \equiv \frac{r_{g0}}{k_x},$$

and

$$\delta_{m0} \equiv \frac{V_{s0}e_*=k_x}{K_x^{-1}}. \tag{16}$$

Here, $\sigma$ is the extracellular inducer concentration, measured in units of $K_x^{-1}$, $\kappa_1$ is the saturation constant for carrier uptake, measured in units of $K_x^{-1}$, $\kappa_1=\kappa_2$ is the ratio of the carrier efflux and influx rates, $\tau_x$ is the ratio of the time constants for diffusive flux ($k_x^{-1}$) and growth on succinate ($r_{g0}^{-1}$), and $\delta_{m0}$ is the ratio of the time constants for diffusive flux ($k_x^{-1}$) and carrier flux in the absence of glucose ($K_x^{-1}=(V_{s0}e_*)$).

Since $r_{g:0} = 0{:}4\,\mathrm{h}^{-1}$, $k_x = 8{:}4\,\mathrm{h}^{-1}$, and $\phi_g$t 2 (see Section 3.1), we obtain $\tau_x\phi_g$t 0:1. It follows that the dilution term in Eq. (12), $\tau_x\phi_g\chi$, is negligibly small compared to the diffusive efflux, $\chi$. Hence, the steady states satisfy the relations

$$0 = \phi_s\delta_{m0} \quad \frac{\sigma=\kappa_1 - \chi=\kappa_2}{1+\sigma=\kappa_1} - (\chi-\sigma), \tag{17}$$

$$= \frac{\phi_{e;lac}}{\phi_g} f(\chi), \tag{18}$$

$$\gamma = \frac{\phi_{e;lac}}{\phi_g} h(\chi), \tag{19}$$

$$\rho = \frac{\phi_{e;gat}}{\phi_g}. \tag{20}$$

We are concerned with the steady states observed in two types of experiments.

If the experiments are performed under conditions that prohibit enzyme synthesis (Fig. 4), the enzyme level is a fixed parameter, and the corresponding steady state intracellular concentration is given by Eq. (17). This equation provides a good fit to the data. Indeed, if we rewrite (17) as

$$(x) = \frac{1}{\phi_s(\delta_{m0}K_x^{-1})} \frac{(x-s)(1+s=K_1)}{s=K_1 - x=K_2} \tag{21}$$

and choose Maloney and Wilson's parameter values, $\phi_s = 1$, $s = 0{:}24\,\mathrm{mM}$, $K_1 = 0{:}8\,\mathrm{mM}$, $K_2 = 84\,\mathrm{mM}$,

$$\delta_{m0}K_x^{-1} = \frac{V_{s0}e_*}{k_x} = \frac{106\,\mathrm{mmol\,min^{-1}\,mL^{-1}}}{0{:}14\,(\mathrm{min}^{-1})} = 760\,\mathrm{mM}, \tag{22}$$

the parametric curve, { (x);x}, shown as the long-dashed curve in Fig. 4, is almost identical to one obtained by Maloney and Wilson.[3]

If the experiments are performed under conditions that permit enzyme synthesis (Fig. 1), the enzyme level is not a fixed parameter. It responds to the prevailing intracellular inducer concentration, and evolves toward the steady state given by (18). The steady state intracellular inducer level is therefore obtained by substituting (18) in (17), which yields

$$0 = \delta_m(G) f(\chi) \frac{\sigma=\kappa_1 - \chi=\kappa_2}{1+\sigma=\kappa_1} - (\chi-\sigma), \tag{23}$$

where

$$\delta_m(G) \equiv \phi(G)\delta_{m0}; \quad \phi(G) \equiv \frac{\phi_s\phi_{e;lac}}{\phi_g}. \tag{24}$$

Thus, $\phi(G)$p 1 captures the cumulative effect of glucose due to inducer exclusion, catabolite repression, and enzyme dilution, and $\delta_m(G)$ is the ratio of the time constant for the diffusive flux relative to the time constant for the carrier flux in the presence of glucose. We are particularly interested in:

(1) The variation of the steady state enzyme activity with the extracellular inducer concentration at any given glucose level (for example, $G = 0$, in Fig. 1a). Since this variation is completely determined by (23), we shall refer to this equation as the equilibrium condition.
(2) The variation of the thresholds with the extracellular glucose concentration (Fig. 1b). These thresholds are the points at which the steady state bifurcates (i.e., changes its stability or multiplicity). It is shown in Appendix A that a steady state bifurcates only if it satisfies the relation

$$1 + \frac{\delta_m}{1+\sigma=\kappa_1} \quad \frac{1}{\kappa_2}(f+\chi f_\chi) - \frac{\sigma}{\kappa_1} f_\chi \quad = 0. \tag{25}$$

We shall refer to this equation as the bifurcation condition.

Thus, the steady states are completely determined by the equilibrium condition, whereas the thresholds must satisfy the equilibrium and bifurcation conditions.

## 3. Results and discussion

### 3.1. The effect of dilution

To simulate the effect of the diffusion influx and the carrier efflux, we need the function, $\phi(G) \equiv \phi_s\phi_e=\phi_g$. In the course of estimating this function, we shall also resolve the discrepancy between the magnitudes of the cAMP-mediated repression reported by Ozbudak et al. and Kuhlman et al.

It follows from (19) and (20) that when the cells are grown in the presence of excess TMG, the ratio of the steady state GFP and RFP intensities is

$$\frac{\gamma}{\rho} = \frac{\phi_{e;lac}(G)}{\phi_{e;gat}(G)}.$$

Since this ratio was observed to be 1 all glucose concentrations (Ozbudak et al., 2004, Fig. 3b), the *lac* and *gat* operons respond identically to CRP–cAMP, i.e.,

$$\phi_{e;lac} = \phi_{e;gat} = \phi_e; \text{ say.} \tag{26}$$

Moreover, the steady state RFP and GFP intensities are given by the equation

$$\rho = \gamma = \frac{\phi_e}{\phi_g}. \tag{27}$$

It follows that the 5-fold decline of $\rho$ at saturating glucose concentrations, shown in Fig. 2, represents the *combined* effect of reduced CRP–cAMP levels *and* enhanced dilution (as opposed to the sole effect of reduced CRP–cAMP levels).

The effect of the reduced CRP–cAMP level, $\phi_e$, cannot be estimated unless the effect of enhanced dilution, $\phi_g$, is known. Ozbudak et al. did not report the specific growth rates at various glucose concentrations, but experiments show that (Narang et al., 1997):

- When *E. coli* K12 is grown on saturating levels of succinate + glucose, the cells consume only glucose during the first exponential growth phase.

[3] Note that even though our expression for the net carrier-mediated influx rate is different from the one used by Maloney and Wilson, we can use their value for $K_1$, since they estimated $K_1$ from initial uptake rates, measured within 30 s of exposure to various extracellular TMG concentrations. Under these conditions, both expressions are identical since $x \approx 0$ during the course of the measurement.

- The maximum specific growth rate on glucose ($0{:}74\,h^{-1}$) is roughly 2 times that on succinate ($0{:}44\,h^{-1}$).

It follows that at saturating glucose concentrations, $\phi_g \approx 2$. Since $\rho \approx \frac{1}{5}$ under these conditions, (27) yields $\phi_e = \rho\phi_g = \frac{2}{5}$. Thus, roughly half of the 5-fold decline in Fig. 2 is due to the enhanced dilution rate at saturating glucose concentrations. Reduction of the CRP–cAMP levels accounts for the remaining 2.5-fold decline, which is consistent with the data obtained by Kuhlman et al.

In view of (27), we can assume that

$$\frac{\phi_e}{\phi_g} = 1 - 0{:}84\frac{G}{7{:}6 + G}, \tag{28}$$

which represents the best fit obtained to the data in Fig. 2b.

It remains to specify the function, $\phi_s$, which characterizes the intensity of inducer exclusion. We assume that the saturation constants for inducer exclusion and cAMP activation/dilution are the same (7:6 mM). Experiments show that the lactose uptake rate decreases 2-fold in the presence of high glucose concentrations (McGinnis and Paigen, 1969, Fig. 3). Thus, we are led to postulate the expression,

$$\phi_s = 1 - 0{:}5\frac{G}{7{:}6 + G}. \tag{29}$$

We shall discuss the implications of the foregoing assumption later on.

### 3.2. The effect of the diffusive influx and carrier efflux

All the parameters required to study the effect of the diffusive influx and carrier efflux are now available (Table 1). Most of the simulations shown below were done with the parameter values for TMG. However, at the end of this section, we shall show the simulation for IPTG, and compare it with the experimental data.

We shall begin by considering the base case of no diffusive influx and no carrier efflux. To this base case, we shall add the diffusive influx and the carrier efflux, one at a time, to examine their effects on the steady states and the thresholds. Finally, we shall show that the general model containing both fluxes is essentially a composite of the two special cases accounting for only one of the two fluxes.

**Table 1**
Parameter values used in the simulations. All the parameter values, except $K_x^{-1}$, are assumed to be the same for TMG and IPTG

| Parameter | Value and reference |
|---|---|
| $K_1$ | 0.8 mM (Maloney and Wilson, 1973) |
| $K_2$ | 84 mM (Fig. 4) |
| $K_x^{-1}$ | 0.47 mM for TMG (Fig. 3a), 0.007 mM for IPTG (Oehler et al., 2006) |
| $\alpha$ | 40 (Oehler et al., 1994) |
| $\beta$ | 1200 (Oehler et al., 1994) |
| $\beta_G$ | 130 (Ozbudak et al., 2004) |
| $\phi_e/\phi_g$ | Eq. (28) |
| $\phi_s$ | Eq. (29) |
| $\delta_{m0}$ | $760/K_x^{-1}$ (Eq. (22)) |

#### 3.2.1. Limiting case 1: no diffusive influx and no carrier influx

In the absence of the diffusive influx and the carrier efflux, the equilibrium condition (23) becomes

$$\chi = \delta_m(G) f(\chi)\frac{\sigma}{\kappa_1 + \sigma}, \tag{30}$$

which can be solved for $\sigma$ to obtain

$$\sigma(\chi; G) = \kappa_1 \frac{\chi}{\delta_m(G) f(\chi) - \chi}. \tag{31}$$

At any fixed $G$, the variation of the steady state , $\gamma$, and $\chi$ with $\sigma$ is therefore given by the parametric curves, $\{\sigma(\chi;G);\ (\chi;G)\}$, $\{\sigma(\chi;G);\ \gamma(\chi;G)\}$, and $\{\sigma(\chi;G);\chi\}$, respectively, where $(\chi;G)$, $\gamma(\chi;G)$, and $\sigma(\chi;G)$ are given by (18), (19), and (31), respectively.

Fig. 7a shows the variation of the steady state and $\gamma$ with $\sigma$ at $G = 0$. The GFP intensity and enzyme activity of the induced cells are identical ($\gamma;\ \approx 1$), but the GFP intensity of non-induced cells is ~7 times their enzyme activity. This can be understood in terms of the variation of the intracellular TMG levels with $\sigma$ (Fig. 7b). In non-induced cells, the intracellular TMG levels are so small compared to $K_x^{-1}$ that the reporter and native *lac* operons are transcribed at their basal rates. Since the basal transcription rate of reporter *lac*, $1/(1 + \alpha + \beta_G) = \frac{1}{170}$, is ~7 times that of native *lac*, $1/(1 + \alpha + \beta) = \frac{1}{1241}$, the GFP intensity of non-induced cells is ~7 times their enzyme activity. In induced cells, on the other hand, the intracellular TMG levels are saturating, and both operons are transcribed at the very same (maximal) rates.

Although the steady state and $\gamma$ have different magnitudes, they have the very same thresholds. Thus, insofar as the thresholds are concerned, it suffices to focus on either one of these variables. Henceforth, we shall confine attention to the enzyme activity.

We are particularly interested in the variation of the thresholds with $G$. However, we shall begin by determining their dependence on $\delta_m$, since this immediately yields the variation with $G$. To this end, observe that in the absence of the carrier efflux, the

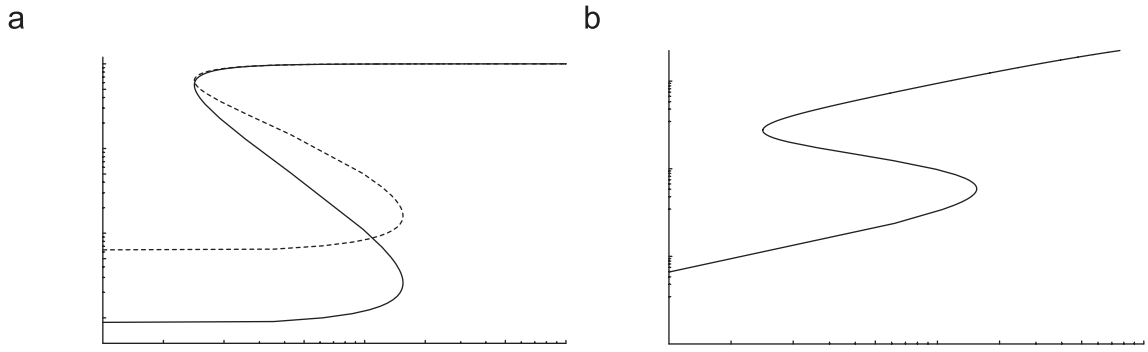


**Fig. 7.** Variation of the steady states with the extracellular TMG level, $\sigma$, at $G = 0$ in the absence of diffusive influx and carrier efflux. (a) Enzyme activity (full line) and green fluorescence intensity (dashed line). (b) Intracellular TMG level.

bifurcation condition (25) becomes

$$1 - \delta_m f_\chi \frac{\sigma}{\kappa_1 + \sigma} = 0. \tag{32}$$

The thresholds satisfy (30) and (32), which imply that $\chi - f \neq f_\chi = 0$. This equation has two positive roots, $\chi_1 o\ \chi_2$, which satisfy the relation, $f_\chi(\chi_1) o\ f_\chi(\chi_2)$ (Appendix B). Hence, the loci of the on and off thresholds are given by the equations

$$\sigma = \frac{\kappa_1}{\delta_m f_\chi(\chi_1) - 1}; \quad \sigma = \frac{\kappa_1}{\delta_m f_\chi(\chi_2) - 1}, \tag{33}$$

respectively, which define two decreasing curves on the $\delta_m\sigma$-plane (Fig. 8a). Moreover, the on and off thresholds are infinitely large when $\delta_m$ approaches $1 \neq f_\chi(\chi_1) = 134$ and $1 \neq f_\chi(\chi_2) = 13{:}4$, respectively, and decrease hyperbolically when $\delta_m \gg 1 \neq f_\chi(\chi_1)$.

Fig. 8a implies that depending on the value of $\delta_m$, there are three different types of dynamics. If $\delta_m 4\ 1 \neq f_\chi(\chi_1)$, there is bistability with finite on and off thresholds (Fig. 7). If $\delta_m o\ 1 \neq f_\chi(\chi_2)$, there is no bistability (Fig. 8b). The bistability disappears because at these $\delta_m$, the intracellular TMG levels are so small compared to $K_x^{-1}$ that $r_e \approx \phi_s f(0)$ is essentially independent of the inducer level, and positive feedback is abolished. If $1 \neq f_\chi(\chi_2) o\ \delta_m o\ 1 \neq f_\chi(\chi_1)$, there is bistability with a finite off threshold, but no on threshold (Fig. 8c). The disappearance of the on threshold is an example of *irreversible bistability* (Laurent and Kellershohn, 1999, p. 421): If enzyme synthesis is switched off by decreasing the extracellular inducer concentration, it can never be switched on by any gradual increase of the extracellular inducer concentration. We shall return to this phenomenon shortly.

The variation of the off and on thresholds with the glucose level, $G$, follows immediately from Fig. 8a. Indeed, as $G$ increases from 0 to 1000 mM, $\delta_m$ decreases from $\delta_{m0}$ to $\delta_{m\infty} \equiv \delta_{m0}\phi|_{G=1000}$ (dotted vertical lines in Fig. 8a). Consequently, the on and off thresholds, and the ratio of the on to off threshold increase. Furthermore, the off threshold exists for all $0 p\ G p\ 1000$ mM, but the on threshold ceases to exist for some $G o\ 1000$ mM.

We can get explicit expressions for the variation of the thresholds with $G$ by letting $\delta_m = \delta_{m0}\phi(G)$ in (33). Since $\phi$ decreases with $G$, $\sigma$ increases with $G$. Thus, on the $G\sigma$-plane, the thresholds are represented by two increasing curves (Fig. 8d). As expected, these curves diverge with increasing glucose levels, with the on threshold becoming unbounded at $G \approx 200$ mM.

### 3.2.2. *Limiting case 2: diffusive influx, but no carrier efflux*

Irreversible bistability is biologically implausible in the case of the *lac* operon. Due to the existence of the diffusive influx, non-induced (and in fact, even cryptic) cells can always be fully induced by exposing them to sufficiently high extracellular inducer levels (Fig. 3a). We show below that irreversible bistability disappears in the presence of the diffusive influx.

In the absence of the carrier efflux, (23) becomes

$$\chi = \sigma + \delta_m(G) f \frac{\sigma}{\kappa_1 + \sigma}, \tag{34}$$

which can be solved for $\sigma$ to obtain

$$\sigma(\chi; G) = \frac{1}{2}\left[-(\kappa_1 + \delta_m f - \chi) + \sqrt{(\kappa_1 + \delta_m f - \chi)^2 + 4\kappa_1\chi}\right]. \tag{35}$$

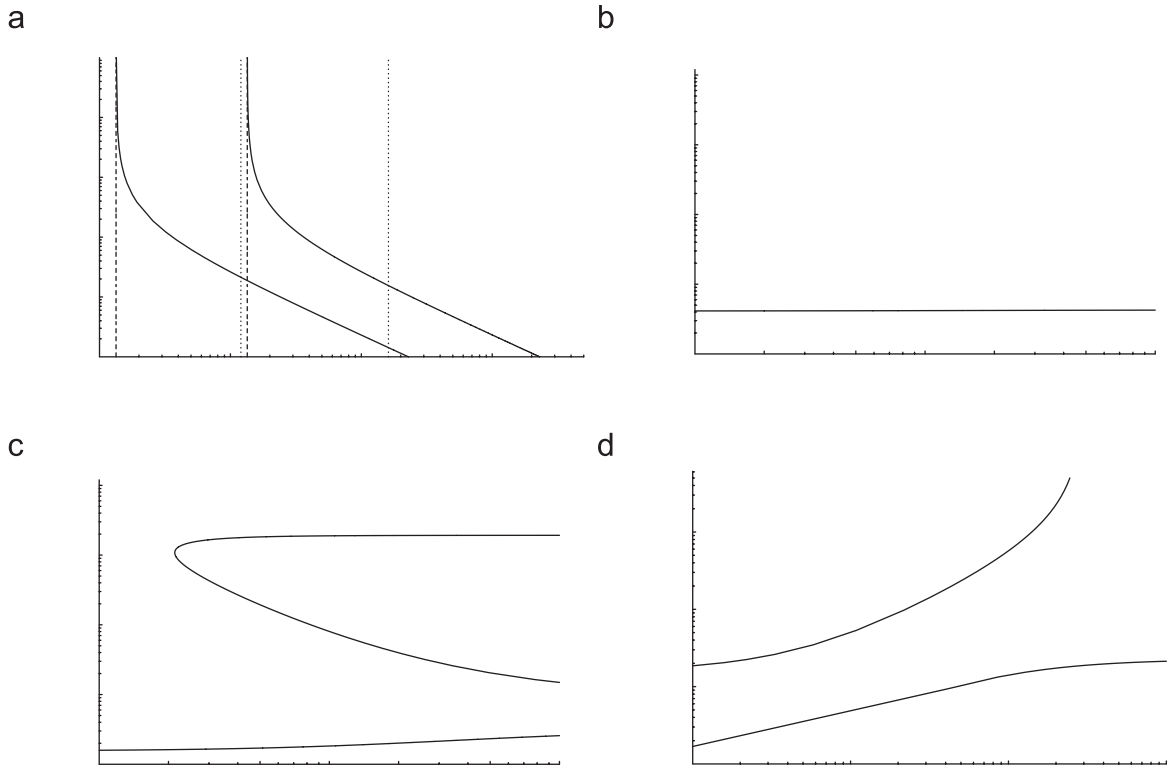


**Fig. 8.** Variation of the on and off thresholds in the absence of diffusive influx and carrier efflux. (a) Variation of the on threshold (upper full curve) and off threshold (lower full curve) with $\delta_m$. The dashed vertical lines represent the values of $\delta_m$ at which the thresholds become infinitely large, namely, $\delta_m = 1 \neq f_\chi(\chi_1) = 134$ and $\delta_m = 1 \neq f_\chi(\chi_2) = 13{:}4$. The dotted vertical lines represent the values of $\delta_m$ at $G = 0$ and 1000 mM. (b) If $\delta_m = 10 o\ 1 \neq f_\chi(\chi_2)$, there is no bistability. (c) If $\delta_m = 80$, which lies between $1 \neq f_\chi(\chi_1)$ and $1 \neq f_\chi(\chi_2)$, there is bistability, but no on threshold. (d) Variation of the off threshold (lower curve) and on threshold (upper curve) with the glucose concentration, $G$. The parameter values in all the figures correspond to those for TMG (see Table 1).

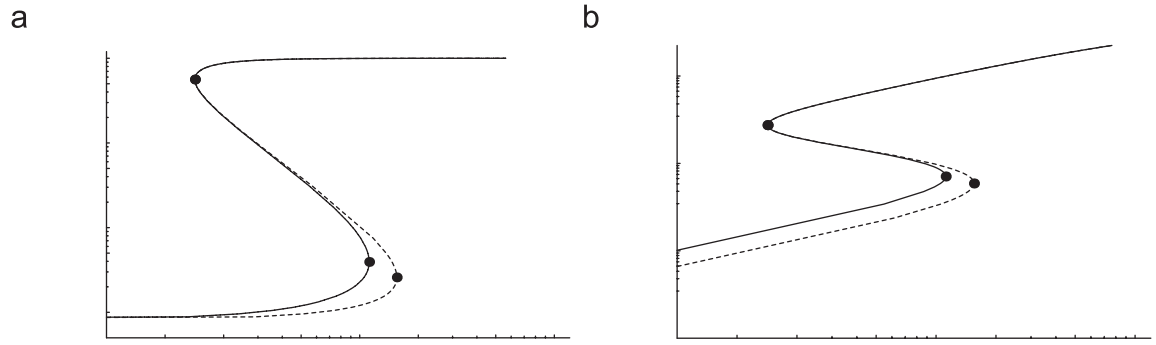


**Fig. 9.** Comparison of the steady states at $G = 0$ in the presence (full lines) and absence (dashed lines) of the diffusive influx. (a) Variation of the steady state permease activity, , with the extracellular TMG level, $\sigma$. (b) Variation of the steady state intracellular TMG concentration, $\chi$, with the extracellular TMG level, $\sigma$.

The variation of the steady state , $\gamma$, and $\chi$ with $\sigma$ is given by the parametric curves, $\{\sigma(\chi;G);\ (\chi;G)\}$ and $\{\sigma(\chi;G);\chi)\}$, respectively, where $(\chi;G)$ and $\sigma(\chi;G)$ are given by (18) and (35), respectively.

Fig. 9a compares the variation of the steady state permease activities with $\sigma$ at $G = 0$ in the presence (full curve) and absence (dashed curve) of the diffusive flux. It is evident that the diffusive flux has no effect on the off threshold, but significantly reduces the on threshold. The physical reason for this is as follows. The off threshold is a steady state associated with induced cells. These cells contain such high permease levels that the diffusive influx makes virtually no contribution to the accumulation of TMG (see upper branches of the curves in Fig. 9b). In contrast, the on threshold is a steady state associated with non-induced cells, which contain such low enzyme levels that the diffusive influx significantly improves the accumulation of TMG (see lower branches of the curves in Fig. 9b). This enhanced accumulation of TMG decreases the on threshold.

We have shown that in the absence of glucose, the diffusive influx has no effect on the off threshold, and decreases the on threshold. This is true even in the presence of glucose. To see this, consider Fig. 10, which compares the thresholds in the presence (full curves) and absence (dashed curves) of the diffusive influx. The full curves correspond to the parametric representation, $\{\delta_m(\chi);\sigma(\chi)\}$, where

$$\sigma(\chi) = \chi - \frac{f}{f_\chi}, \tag{36}$$

$$\delta_m(\chi) = \frac{1}{f_\chi}\ 1 + \frac{\kappa_1}{\sigma(\chi)} \tag{37}$$

are obtained by solving (32) and (34) for $\sigma$ and $\delta_m$. It is evident from the figure that over the range, $\delta_{m\infty}$p $\delta_m$p $\delta_{m0}$, the off thresholds in the presence of the diffusive influx (lower full curve) coincide with the off thresholds in absence of the diffusive influx (lower dashed curve). However, the on thresholds in the presence of the diffusive influx (upper full curve) are significantly smaller than the on thresholds in the absence of the diffusive flux (upper dashed curve). Thus, as $G$ increases to 02 1000 mM, both thresholds increase, but the ratio of the on to off threshold decreases (in contrast to the increase observed in the absence of diffusive flux).

When $\delta_m \gtrsim 2000$, the diffusive influx has no effect on both thresholds. Under these conditions, even the non-induced cells have such high permease activities that the diffusive influx makes no contribution to inducer accumulation.

When $\delta_m$t 50, the diffusive flux has a significant effect on both thresholds. Under these conditions, even the induced cells have

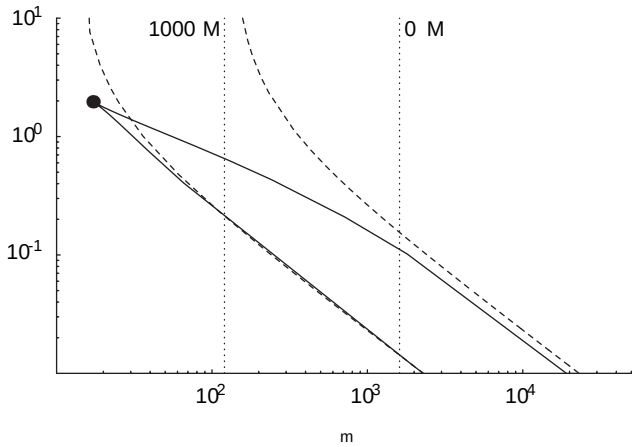


**Fig. 10.** Comparison of the thresholds at various $\delta_m$ in the presence and absence of the diffusive influx. The lower and upper full curves, defined by (36) and (37), represent the off and on thresholds, respectively, in the presence of the diffusive influx. The full circle shows the cusp at which the thresholds merge. The lower and upper dashed curves, defined by (33), represent the off and on thresholds, respectively, in the absence of the diffusive influx. The dotted vertical lines show the values of $\delta_m \equiv \delta_{m0}\phi(G)$ at $G = 0$ and 1000 mM. The parameter values correspond to those for TMG (see Table 1).

low permease activities. Hence, the diffusive flux contributes significantly to inducer accumulation in both non-induced and induced cells. At sufficiently small $\delta_m$, the inducer accumulates almost entirely by diffusion, i.e., $\chi \approx \sigma$. Since the intracellular TMG level is independent of the enzyme level, there is no positive feedback, and hence, no bistability (manifested in Fig. 10 by the formation of a cusp at which the two thresholds merge).

The existence of the cusp implies that bistability is reversible whenever it exists: Either both or none of the thresholds occur at any given $\delta_m$. Irreversible bistability, which is characterized by the existence of only one of the thresholds, disappears in the presence of the diffusive flux. This conclusion does not depend on the precise parameter values or the functional form of $f(\chi)$. The shape of the curves in Fig. 10 is independent of these details, as long as the induction kinetics are sigmoidal (Appendix C).

### 3.2.3. *Limiting case 3: carrier efflux, but no diffusive influx*

In this case, (23) becomes

$$\chi = \delta_m(G) f \frac{\sigma/\kappa_1 - \chi/\kappa_2}{1 + \sigma/\kappa_1}, \tag{38}$$

which can be solved for $\sigma$ to obtain

$$\sigma(\chi;G) = \kappa_1 \frac{\chi[1=(\delta_m f) + 1=\kappa_2]}{1 - \chi=(\delta_m f)}. \tag{39}$$

The variation of the steady state and $\chi$ with $\sigma$ is given by the parametric curves, $\{\sigma(\chi;G);\ (\chi;G)\}$, and $\{\sigma(\chi;G);\chi)\}$, respectively, where $(\chi;G)$ and $\sigma(\chi;G)$ are given by (18) and (39), respectively.

Fig. 11a shows the variation of the enzyme activity with $\sigma$ at $G = 0$ in the presence (full curve) and absence (dashed curve) of the carrier influx. Evidently, the carrier efflux has no effect on the on threshold, but it significantly increases the off threshold. This is because in non-induced cells, the intracellular TMG levels are so small compared to $K_2$ that carrier efflux is negligible (Fig. 11b). However, induced cells, characterized by relatively high intracellular TMG levels, suffer from pronounced carrier efflux, which increases their off threshold.

Fig. 12 compares the thresholds in the presence of carrier efflux (full curves) with those obtained in its absence (dashed curves). The full curves were obtained by plotting the parametric representation, $\{\delta_m(\chi);\sigma(\chi)\}$, where

$$\delta_m(\chi) = \frac{1}{f^2}[\kappa_2(\chi f_\chi - f) + \chi^2 f_\chi], \tag{40}$$

$$\sigma(\chi) = \frac{\kappa_1}{\kappa_2}\frac{\chi^2 f_\chi}{\chi f_\chi - f} \tag{41}$$

are the solutions of (38) and (25). It is evident that over the range, $\delta_{m\infty} \leq \delta_m \leq \delta_{m0}$, the carrier efflux has no effect on the on threshold, but significantly reduces the off threshold. Thus, the behavior observed in the presence of glucose is identical to that observed in the absence of glucose. When $\delta_m \gtrsim 10^4$, both thresholds are affected by the carrier efflux because the enzyme activity is so large that even the non-induced cells experience carrier efflux. At sufficiently large $\delta_m$, the thresholds merge to form a cusp, beyond which there is no bistability. The bistability disappears because under these conditions, the intracellular TMG level is $\chi \approx (\kappa_2=\kappa_2)\sigma$, which is independent of the enzyme level. The destabilizing effect of positive feedback therefore vanishes, and the prospect of bistability is eliminated.

Once again, the qualitative variation of the thresholds with $G$ can be inferred from Fig. 12. As $G$ increases, so do both thresholds and the ratio of the on to off threshold. Furthermore, since diffusive influx is absent, there is irreversible bistability: The off threshold exists for all $G$, whereas the on threshold disappears at some $G \approx 1000$ mM.

We note finally that the geometry of the bifurcation curves in Fig. 12 is independent of the parameter values, provided the induction rate is sigmoidal (Appendix D).

### 3.2.4. General case: diffusive influx and carrier efflux

Intuition suggests that the behavior of the full model can be inferred from the behavior of limiting cases 2 and 3. To see this, it suffices to recall that the on threshold is a steady state associated with non-induced cells. Since carrier efflux is negligible in such cells, the on thresholds of the full model will be identical to the on thresholds for limiting case 2 (no carrier efflux). Likewise, the off threshold is associated with induced cells. Since diffusive influx is negligible in such cells, the off thresholds of the full model will be identical to the off thresholds for limiting case 3 (no diffusive influx). We show below that this is indeed the case.

Fig. 13 compares the steady state profiles at $G = 0$ in the presence of the diffusive influx and carrier efflux (full curves) with those obtained in the presence of the diffusive influx only (short-dashed curves) and the carrier efflux only (long-dashed curves). The full curves were obtained from the parametric representation,

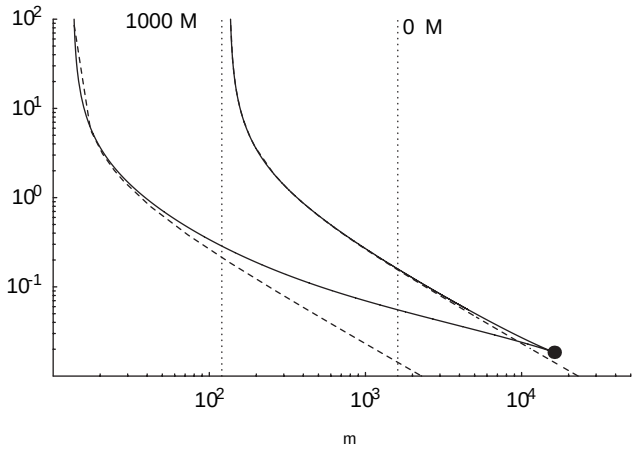


**Fig. 12.** Comparison of the thresholds at various $\delta_m$ in the presence and absence of the carrier efflux. The lower and upper full curves, defined by (40) and (41), represent the off and on thresholds, respectively, in the presence of the carrier efflux. The full circle shows the cusp at which the thresholds merge. The lower and upper dashed curves, defined by (33), represent the off and on thresholds, respectively, in the absence of the carrier efflux. The dotted vertical lines show the values of $\delta_m \equiv \delta_{m0}\phi(G)$ at $G = 0$ and 1000 mM. The parameter values correspond to those for TMG (see Table 1).

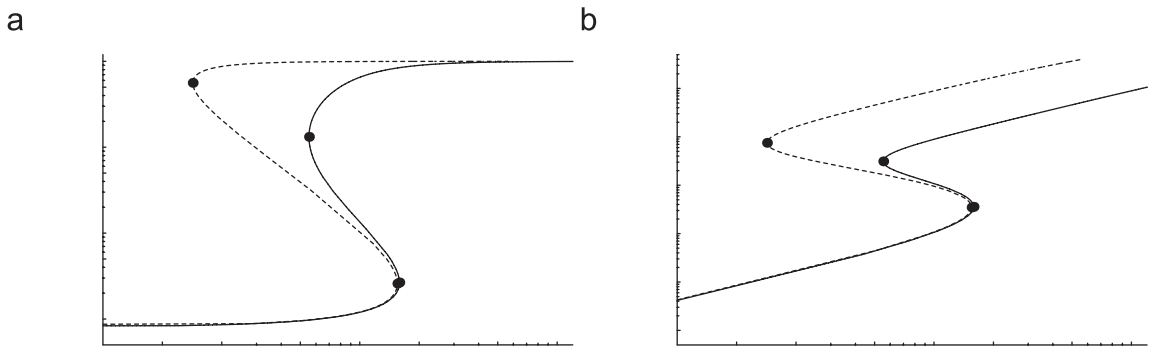


**Fig. 11.** Comparison of the steady states at $G = 0$ in the presence (full lines) and absence (dashed lines) of the carrier efflux. (a) Variation of the steady state enzyme activity with the extracellular TMG level. (b) Variation of the intracellular TMG concentration with the extracellular TMG level.

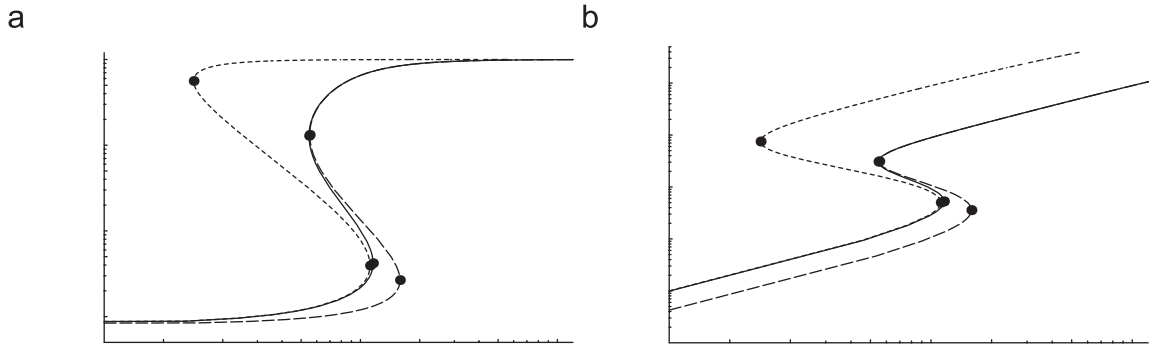


**Fig. 13.** Comparison of the steady states of the general model (full curves) with the steady states in the presence of diffusive flux (short-dashed curves) and carrier efflux (long-dashed curves). (a) Variation of the enzyme activity with the extracellular TMG level. (b) Variation of the intracellular TMG concentration with the extracellular TMG level.

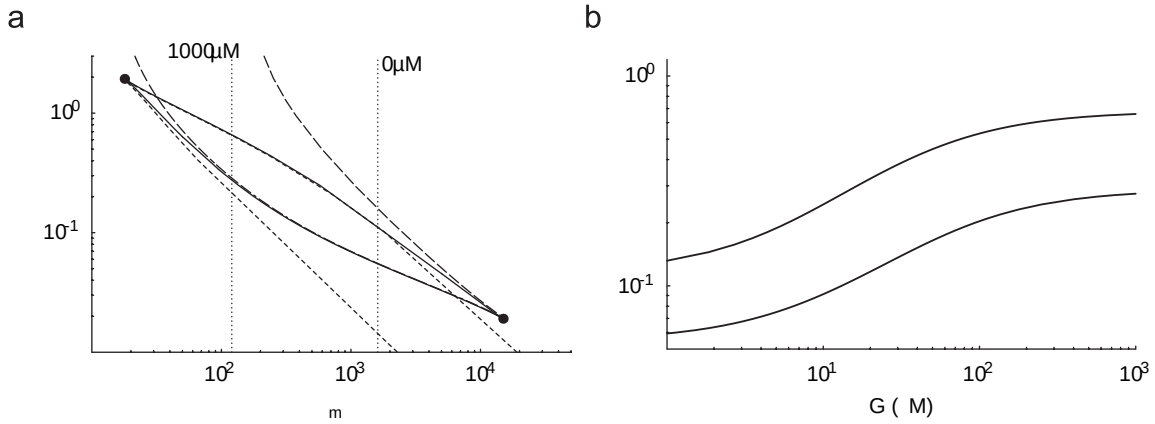


**Fig. 14.** Variation of the thresholds in the presence of both fluxes. (a) Variation of the thresholds with $\delta_m$. The lower and upper full curves, defined by (43) and (44), represent the off and on thresholds, respectively, in the presence of both fluxes. The full circles show the cusps at which the thresholds merge. The short-dashed curves, defined by (36) and (37), represent the thresholds in the presence of the diffusive influx only. The long-dashed curves, defined by (40) and (41), represent the thresholds in the presence of the carrier efflux only. The dotted vertical lines show the values of $\delta_m \equiv \delta_{m0}\phi(G)$ at $G = 0$ and 1000 mM. (b) Variation of the thresholds with the glucose concentration, $G$. The parameter values in both figures correspond to those for TMG (see Table 1).

$\{\sigma(\chi;G);\ (\chi;G)\}$ and $\{\sigma(\chi;G);\chi)\}$, where

$$\sigma(\chi;G) = \frac{\kappa_1}{2}\left(-p + \sqrt{p^2 + 4\frac{\chi}{\kappa_1}\left(1+\frac{\delta_m f}{\kappa_2}\right)}\right);\quad p \equiv 1 - \frac{\chi}{\kappa_1} + \frac{\delta_m f}{\kappa_1} \tag{42}$$

is the positive solution of (23), and $(\chi;G)$ is given by (18). It is evident that the on (resp., off) threshold is well approximated by the model accounting for only the diffusive flux (resp., carrier efflux).

The above conclusion is true for all glucose concentrations. Fig. 14a compares the thresholds thus obtained (full curves) with the thresholds obtained in the presence of diffusive influx (short-dashed curves) and carrier efflux (long-dashed curves). The full curves were generated from the parametric representation, $\{\delta_m(\chi);\sigma(\chi)\}$, where $\delta_m(\chi);\sigma(\chi)$ satisfy the relations

$$0 = \sigma^2 + \sigma\left(\frac{f}{f_\chi} - \left(\chi + \frac{\kappa_1}{\kappa_2}\frac{f+\chi f_\chi}{f_\chi}\right)\right) - \frac{\kappa_1}{\kappa_2}\chi^2, \tag{43}$$

$$\delta_m = \frac{1+\sigma/\kappa_1}{f_\chi\sigma/\kappa_1 - (\chi f_\chi + f)/\kappa_2}, \tag{44}$$

obtained from (23) and (25). Unlike the cases discussed above, the thresholds exist only on a finite interval—they terminate in a cusp at both small and large $\delta_m$. Moreover, over the range, $\delta_{m\infty} \lesssim \delta_m \lesssim \delta_{m0}$, the on (resp., off) thresholds are well approximated by the on (resp., off) thresholds in the presence of only the diffusive flux (resp., carrier efflux).

It follows from Fig. 14a that as $G$ increases, both thresholds increase, but the ratio of on to off thresholds can increase, decrease, or pass through a maximum. For the parameter values in Table 1, $\delta_{m0}$ and $\delta_{m\infty}$ are such that the ratio passes through a maximum. The precise variation of the thresholds with $G$ is given by the parametric curve, $\{G(\chi);\sigma(\chi)\}$, where

$$G(\chi) = \phi^{-1}\left(\frac{1}{\delta_{m0}}\frac{1+\sigma/\kappa_1}{f_\chi\sigma/\kappa_1 - (\chi f_\chi + f)/\kappa_2}\right).$$

As expected, this parametric curve consists of two increasing curves that diverge at low glucose concentrations and converge at high glucose concentrations (Fig. 14b).

### 3.2.5. Comparison of simulations with the data for TMG

Comparison of the model simulations (dashed lines in Fig. 1b) with the data shows that the simulated off thresholds are higher, and the simulated on thresholds are lower, than the corresponding thresholds observed experimentally. Moreover, the off threshold is most discrepant at low glucose concentrations, whereas the on threshold deviates at high glucose concentrations.

Part of the discrepancy is due to uncertainties in the parameter values. Indeed, the value of $K_2$ is based on a fit of the data rather than a direct measurement. Moreover, even the measured values in Table 1 were obtained with different strains of *E. coli*, and there is considerable variation depending on the strain. The value of $K_1$, for instance, is 0.43 mM in *E. coli* ML30 (Cohen and Monod, 1957, Fig. 2), and 0.8 mM in *E. coli* K12 CA6008 (Maloney and Wilson, 1973). However, there may be two additional sources of the discrepancy.

*Dependence of $\phi_s$ on the enzyme activity*: The model assumes that the effect of inducer exclusion, characterized by the function $\phi_s$, is completely determined by the extracellular glucose level. However, the data in Fig. 15 implies that $\phi_s$ also depends on the activity of the permease. Inducer exclusion is significant in cells containing low enzyme levels, but disappears in fully induced cells presumably because enzyme $IIA^{glc}$ binds to only a small fraction of the abundant permease (Mitchell et al., 1982).

The model, which ignores the dependence of $\phi_s$ on the permease level, yields a good fit to the data obtained in the absence of α-methylglucoside (full line in Fig. 15). However, in the presence of α-methylglucose, it fits the data well only if the enzyme levels are high—it underestimates the inducer exclusion effect at low enzyme levels (dashed line in Fig. 15). The observed on threshold is therefore expected to be higher than the on threshold predicted by the model.

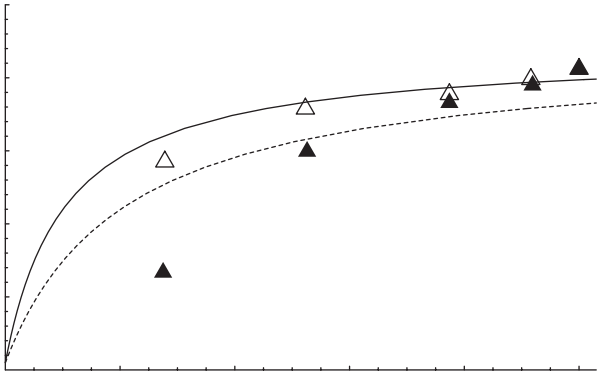

**Fig. 15.** Comparison of the observed and simulated effects of inducer exclusion in *S. typhimurium* SB3939 transfected with a plasmid encoding the *lac* operon (Mitchell et al., 1982, Fig. 5A). The open triangles show the steady state intracellular TMG level in cells induced to various levels, and exposed to a carbon-free medium containing 1 mM TMG. The full triangles show the intracellular TMG level attained in a carbon-free medium containing 1 mM TMG and 10 mM α-methylglucoside, a non-metabolizable analog of glucose. The full curve shows the fit to the data obtained with Eq. (21) and the parameter values, $\delta_{m0}K_x^{-1} = 760\,\text{mM}$, $\phi_s|_{G=0} = 1$, $k_x = 0{:}14\,\text{min}^{-1}$, $s = 1\,\text{mM}$, $K_1 = 0{:}8\,\text{mM}$, and $K_2 = 35\,\text{mM}$. The dashed curve shows the fit to the data with the same equation and parameter values, the only difference being that $\phi_s|_{G=10\,\text{mM}} = 0{:}5$.

The dependence of $\phi_s$ on the enzyme activity can explain the discrepancy of the on threshold, which is most pronounced at large glucose concentrations. However, it cannot account for the discrepancy in the off threshold, which is largest at low glucose concentrations. As we show below, this discrepancy can be resolved by a process that is significant even in the absence of glucose.

*Dependence of $r_{g;0}$ on the enzyme activity*: The model assumes that in the absence of glucose, the specific growth rate is a fixed constant, $r_{g;0}$. However, the data shows that the specific growth rate varies significantly with the enzyme level of the cells (Fig. 16a). When the cells are exposed to 0.5 mM TMG, the specific growth rate is ~30% lower than that of non-induced cells, and the graph suggests that the specific growth rate declines further at higher extracellular TMG levels. The reduced specific growth rate of the induced cells serves to decrease the off threshold because the lower the specific growth rate, the higher the enzyme and intracellular TMG levels.

In earlier work, we studied the dynamics of growth on lactose (Narang and Pilyugin, 2008). There, we showed that bistability is suppressed during growth on lactose because the specific growth rate increases with the enzyme level, thus enhancing the stabilizing effect of dilution. Since the specific growth rate decreases with the enzyme level during growth on TMG, it is plausible to expect that in this case, the stabilizing effect of dilution is depressed, and the bistable regime is enlarged.

### 3.2.6. Comparison of simulations with the data for IPTG

The above arguments suggest that the discrepancy between the data and the simulations would be reduced if the experiment was performed in the absence of glucose with a gratuitous inducer that does not result in a significant reduction of the specific growth rate. This conclusion seems to be consistent with the data.

It turns out that when the cells are grown in the presence of IPTG, the specific growth rate of the induced cells is only ~5% smaller than the specific growth rate of the non-induced cells (Fig. 16b). Recently, Laurent et al. measured the variation of the enzyme activity with the extracellular IPTG levels in the absence of glucose (Fig. 17). They found that the mean activity does not

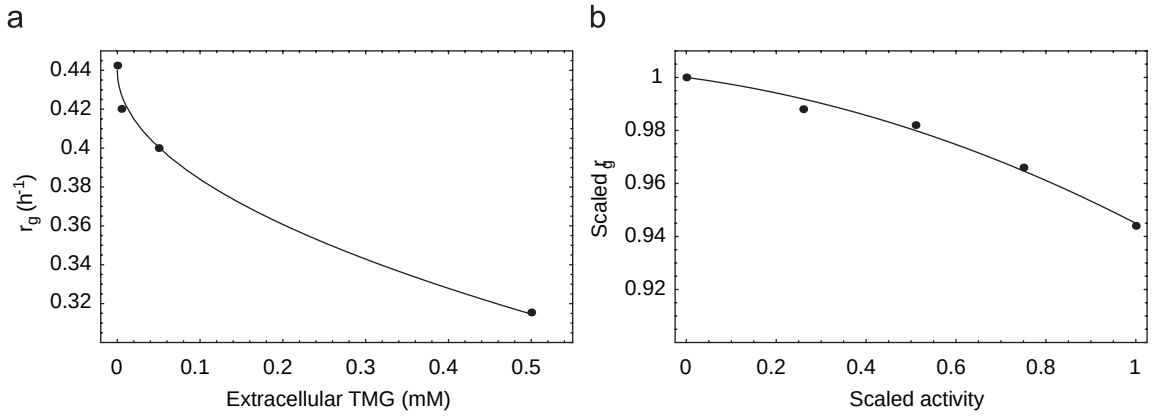


**Fig. 16.** Variation of the specific growth rate due to induction of *lac*. (a) During growth of *E. coli* B in the presence of succinate and TMG, full induction of the cells reduces the specific growth rate by ~30% (Novick and Weiner, 1957, Table 2). (b) During growth of *E. coli* K12 MG1655 in the presence of glycerol and IPTG, full induction reduces the specific growth rate by only ~5% (Dekel and Alon, 2005, Fig. 2a).

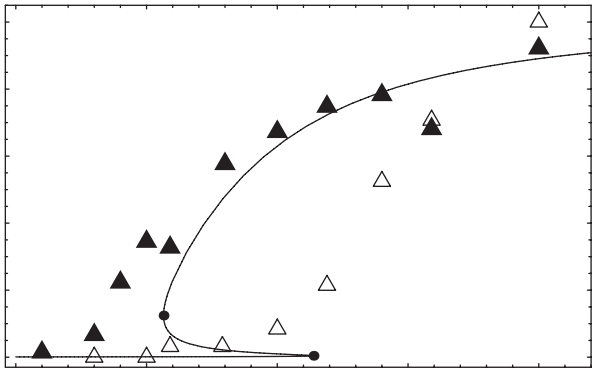

**Fig. 17.** Comparison of the data and model simulation for bistability of *E. coli* K12 at various extracellular IPTG levels and $G = 0$. The open and closed triangles show the steady state $\beta$-galactosidase activities of non-induced and induced cells, respectively (Laurent et al., 2005, Fig. 7). The full curve shows the model simulation with $K_x^{-1} = 7\,\text{mM}$. All other parameter values are the same as those used for simulating the experiments with TMG (see Table 1).

display the discrete all-or-none response observed by Ozbudak et al. (presumably due to the physiological heterogeneity of the cells and the inherent stochasticity of the induction process). However, there is clear evidence of bistability in the 5-fold range, 0:32 1:5 mM, which is significantly smaller than the 10-fold range shown in Fig. 1a. The off and on thresholds are also smaller than those observed by Ozbudak et al. (0.3 and 1:5 mM compared to 3 and 30 mM in Fig. 1a). This is because the affinity of IPTG for the repressor is an order of magnitude higher than that for TMG. Simulation of the model with $K_x^{-1} = 7\,\text{mM}$ yields results that are in reasonable agreement with the data (Fig. 17).

It is important to note that even though the modifications mentioned above may be necessary to resolve the quantitative discrepancy, they will have no effect on the key phenomenon predicted by the model, namely, the disappearance of bistability at low and high values of the permease activity. Indeed, the mere existence of diffusive influx and carrier influx implies that at sufficiently low and high permease activities, the intracellular inducer level becomes independent of the permease activity, thus eliminating positive feedback and bistability. This prediction can be tested by studying the enzyme distribution in (a) wild-type cells exposed to specific permease inhibitors such as *p*-chloromercuribenzene sulfonate (Booth and Hamilton, 1980), or mutants with impaired *lac* induction (Maloney and Wilson, 1973) and (b) recombinant cells overexpressing the permease (Kimata et al., 1997).

## 4. Conclusions

Analysis of the experimental data shows that the diffusive influx and carrier efflux have a profound effect on inducer accumulation in non-induced and induced cells, respectively. Since bistability entails the coexistence of steady states corresponding to both non-induced and induced cells, neither one of these fluxes can be neglected. We analyzed a model of *lac* bistability taking due account of the diffusive influx and carrier efflux. We find that:

(1) The 5-fold CRP–cAMP mediated repression reported by Ozbudak et al. is almost 2 times the repression observed by others. This discrepancy can be resolved by accounting for the enhanced dilution effect in the presence of glucose. Our analysis shows that half of the 5-fold repression reported by Ozbudak et al. is due to dilution.
(2) The diffusive influx decreases the on threshold, and eliminates irreversible bistability, a phenomenon that is inconsistent with experiments. The carrier efflux increases the off threshold, and abolishes the prospect of bistability at large permease levels. Thus, the model predicts the disappearance of bistability at both small and large permease levels.
(3) Over a wide range of permease activities, the diffusive influx has no effect on the off threshold, and the carrier efflux has no effect on the on threshold. Since each of these fluxes influences only one of the thresholds, the thresholds in the presence of both fluxes can be approximated by simple analytical expressions corresponding to two limiting cases, namely, no diffusive influx and no carrier efflux.
(4) Simulations of the model show good agreement with the data for IPTG. They are discrepant with respect to the data for TMG. The discrepancy is probably due to uncertainties in the parameter values, or the absence of certain features in the model, such as the dependence of the inducer exclusion effect and the specific growth rate on the prevailing lactose enzyme levels.

## Acknowledgments

This research was supported in part with funds from the National Science Foundation under Contract NSF DMS-0517954. We are grateful to Stefan Oehler (IMBB-FoRTH) for discussions regarding the regulation of the *lac* operon.

## Appendix A. Necessary condition for a bifurcation

The Jacobian of Eqs. (12)–(15) at any steady state is

$$\begin{bmatrix} -\frac{1}{\tau_x}\left(\frac{\phi_s\delta_{m0}(\phi_s=\phi_g)f}{\kappa_2(1+\sigma=\kappa_1)}+1+\tau_x\phi_g\right) & \frac{\phi_s\delta_{m0}}{\tau_x}\left(\frac{\sigma=\kappa_1-\chi=\kappa_2}{1+\sigma=\kappa_1}-\frac{\chi}{\kappa_2}\right) & 0 & 0 \\ \phi_e f_\chi & -\phi_g & 0 & 0 \\ \phi_e h_\chi & 0 & -\phi_g & 0 \\ 0 & 0 & 0 & -\phi_g \end{bmatrix}.$$

Evidently, two of the eigenvalues are $-\phi_g$. Hence, the steady state is stable if and only if the remaining two eigenvalues corresponding to the submatrix

$$\begin{bmatrix} -\frac{1}{\tau_x}\left(\frac{\phi_s(\phi_s=\phi_g)\delta_{m0}f}{\kappa_2(1+\sigma=\kappa_1)}+1+\tau_x\phi_g\right) & \frac{\phi_s\delta_{m0}}{\tau_x}\left(\frac{\sigma=\kappa_1-\chi=\kappa_2}{1+\sigma=\kappa_1}\right) \\ \phi_e f_\chi & -\phi_g \end{bmatrix}$$

have negative real parts. Since the trace is always negative, stability results whenever the determinant is positive. Hence, the necessary condition for a bifurcation is that the determinant be zero, i.e.,

$$\frac{\phi_g}{\tau_x}\left\{\phi_s\left(\frac{\phi_s=\phi_g}{\kappa_2(1+\sigma=\kappa_1)}\delta_{m0}f+1+\tau_x\phi_g\right)\right\} = \frac{\phi_s\phi_e\delta_{m0}f_\chi}{\tau_x}\left(\frac{\sigma=\kappa_1-\chi=\kappa_2}{1+\sigma=\kappa_1}\right).$$

Since $\tau_x\phi_g \ll 1$, this condition can be approximated by the relation

$$1+\frac{\delta_m f}{\kappa_2(1+\sigma=\kappa_1)}-\frac{\delta_m f_\chi}{1+\sigma=\kappa_1}\left(\frac{\sigma}{\kappa_1}-\frac{\chi}{\kappa_2}\right)=0; \quad \delta_m \equiv \frac{\phi_s\phi_e}{\phi_e}\delta_{m0},$$

which immediately reduces to Eq. (25).

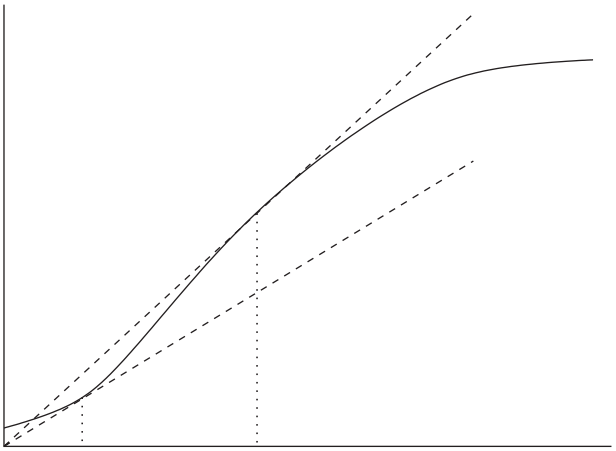

**Fig. B1.** There are exactly two lines passing through the origin (dashed lines) that are tangential to the graph of $f$ (full curve). The slopes of these lines are $f(\chi_1)/\chi_1 = f_\chi(\chi_1)$ and $f(\chi_2)/\chi_2 = f_\chi(\chi_2)$.

## Appendix B. The positive roots of the equation $\chi - f/f_\chi = 0$

We wish to show that $q(\chi) \equiv \chi - f/f_\chi$ has exactly two positive roots, $\chi_1 \geq \chi_2$, and is positive if and only if $\chi_1 \geq \chi \geq \chi_2$. This assertion has a simple geometric interpretation. Since $f(\chi)$ is a sigmoidal function for sufficiently large $\alpha$ and $\hat{\alpha}$, there are only two lines passing through the origin that touch the graph of $f$, and they do so at the two points, $\chi_1$ and $\chi_2$ (Fig. B1). Furthermore, for any $\chi_1 \geq \chi \geq \chi_2$, the slope of the line passing through $(0;0)$ and $(\chi;f(\chi))$ is smaller than $f_\chi$.

The formal proof is obtained by observing that $q(0) = -f(0)/f_\chi(0) \leq 0$, and at large $\chi$,

$$q(\chi) = \chi - \frac{1+\chi}{2}\frac{1+\alpha/(1+\chi)^2+\hat{\alpha}/(1+\chi)^4}{\alpha/(1+\chi)^2+2\hat{\alpha}/(1+\chi)^4} \approx \chi - \frac{\chi}{2}\frac{1}{\alpha/\chi^2} \geq 0.$$

It follows that $q(\chi)$ has at least two positive roots. In fact, it has exactly two positive roots because it has only one extremum on $[0;\infty)$. Indeed,

$$\frac{dq}{d\chi} = 1 - \frac{f_{\chi\chi}f - f_\chi^2}{f_\chi^2} = \frac{f_{\chi\chi}f}{f_\chi^2},$$

which is zero if and only if $f_{\chi\chi} = 0$, i.e., $\chi = \chi_*$, where $(\chi_*;f(\chi_*))$ is the unique inflection point of the sigmoidal function, $f$.

## Appendix C. Bifurcation diagram for diffusive influx

We wish to show that regardless of the parameter values, the functions, $\sigma(\chi)$ and $\delta_m(\chi)$, defined by (36) and (37), respectively, have the geometry shown in Fig. C1. It follows that as $\chi$ increases from $\chi_1$, $\sigma$ increases and $\delta_m$ decreases until a cusp forms at the point $\chi = \chi_*$ where $d\sigma/d\chi = d\delta_m/d\chi = 0$. Beyond $\chi = \chi_*$, $\sigma$ decreases and $\delta_m$ increases until they approach 0 and $\infty$, respectively. Thus, the variation of the thresholds on the $\delta_m\sigma$-plane has the geometry shown in Fig. 10a, regardless of the parameter values.

Now, the geometry of $\sigma(\chi)$ is identical to that of $q(\chi)$, which was analyzed in Appendix B. Hence, it suffices to show that $\delta_m(\chi)$ has the geometry shown in Fig. C1. To this end, observe that (37)

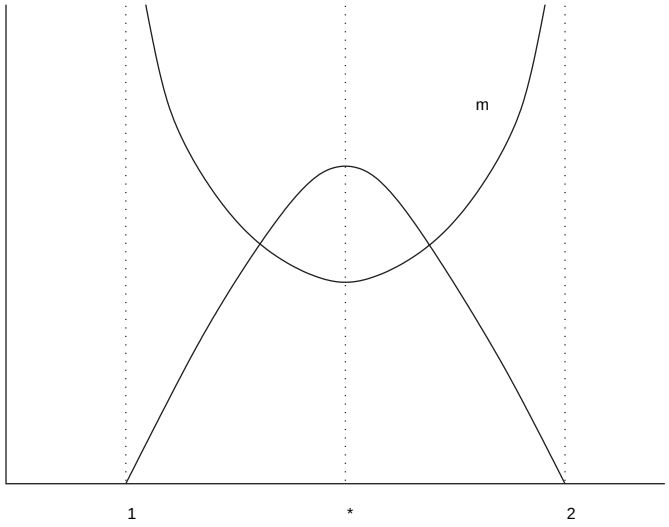


**Fig. C1.** Geometry of the $\delta_m(\chi)$ and $\sigma(\chi)$ in the case of diffusive influx.

implies $\lim_{\chi\to\chi_1^+;\chi_2^-}\delta_m(\chi) = \infty$. Moreover, since

$$\frac{d\delta_m}{d\chi} = -\frac{\kappa_1}{\sigma^2 f_\chi}\frac{d\sigma}{d\chi} - \left(1+\frac{\kappa_1}{\sigma}\right)\frac{f_{\chi\chi}}{f_\chi^2}$$
$$= -\frac{d\sigma}{d\chi}\left(\frac{\kappa_1}{\sigma^2 f_\chi} + \left(1+\frac{\kappa_1}{\sigma}\right)\frac{1}{f}\right),$$

$d\delta_m/d\chi$ and $d\sigma/d\chi$ have opposite signs at all $\chi_1 \geq \chi \geq \chi_2$, except when $\chi = \chi_*$, at which point $d\delta_m/d\chi = d\sigma/d\chi = 0$.

## Appendix D. Bifurcation diagram for carrier influx

In this case, the equilibrium and bifurcation conditions have the form

$$\chi\left(1+\frac{\sigma}{\kappa_1}\right) - \delta_m f\frac{\sigma}{\kappa_1} = 0, \tag{D.1}$$

$$1+\frac{\sigma}{\kappa_1} - \delta_m\left(\frac{1}{\kappa_2}(f+\chi f_\chi) - \frac{\sigma}{\kappa_1}f_\chi\right) = 0. \tag{D.2}$$

Differentiating (D.1) and using (D.2), we find that

$$\frac{1}{\kappa_1}(\delta_m f - \chi)\frac{d\sigma}{d\chi} + f\left(\frac{\sigma}{\kappa_1} - \frac{\chi}{\kappa_2}\right)\frac{d\delta_m}{d\chi} = 0, \tag{D.3}$$

where the coefficients of $d\sigma/d\chi$ and $d\delta_m/d\chi$ are positive because (D.1) implies that

$$\delta_m f - \chi = \frac{\chi\kappa_1}{\sigma} \geq 0,$$

and (D.2) yields

$$\frac{\sigma}{\kappa_1} - \frac{\chi}{\kappa_2} = \frac{1+\frac{\sigma}{\kappa_1}+\frac{\delta_m f}{\kappa_2}}{\delta_m f_\chi} \geq 0.$$

We conclude that either $d\sigma/d\chi$ and $d\delta_m/d\chi$ have opposite signs or they are both simultaneously equal to zero. Thus, the parametric curve described by (D.1) and (D.2) is piece-wise smooth, and consists of several cusps connected by graphs of monotonically decreasing functions in the $\delta_m;\sigma$-plane.

It turns out that the parametric curve has only one cusp. Indeed, $\sigma(\chi)$ and $\delta_m(\chi)$ are given by Eqs. (40) and (41), respectively. We will show that $\sigma(\chi)$ admits a unique minimum on the interval $[\chi_1;\chi_2]$ where it is positive. For convenience,

we rewrite the expression for $\sigma(\chi)$ as

$$\sigma(\chi) = \frac{\kappa_1}{\kappa_2}\frac{\chi^2 f_\chi}{\chi f_\chi - f} = \frac{\kappa_1}{\kappa_2}\frac{\chi^2 f_\chi / f^2}{\chi f_\chi / f^2 - 1/f} = \frac{\kappa_1}{\kappa_2}\frac{\chi^2 g_\chi}{\chi g_\chi + g},$$

where

$$g(\chi) = \frac{1}{f(\chi)} = 1 + \frac{\alpha}{(1+\chi)^2} + \frac{\hat{\alpha}}{(1+\chi)^4}.$$

Differentiating with respect to $\chi$ and simplifying, we find that

$$\frac{d\sigma}{d\chi} = \frac{\kappa_1}{\kappa_2}\frac{2\chi g g_\chi + \chi^2 g g_{\chi\chi}}{(\chi g_\chi + g)^2} = \frac{\kappa_1 \chi g}{\kappa_2(\chi g_\chi + g)^2}(2g_\chi + \chi g_{\chi\chi}).$$

Hence the sign of $d\sigma/d\chi$ is determined by the sign of $h(\chi) \equiv 2g_\chi + \chi g_{\chi\chi}$. Letting $z = 1 + \chi$, we find that

$$\begin{aligned} h(z) &= -\frac{4\alpha}{z^3} - \frac{8\hat{\alpha}}{z^5} + (z-1)\left(\frac{6\alpha}{z^4} + \frac{20\hat{\alpha}}{z^6}\right) \\ &= \frac{2\alpha z^3 - 6\alpha z^2 + 12\hat{\alpha} z - 20\hat{\alpha}}{z^6}. \end{aligned} \tag{D.4}$$

The numerator of this expression is negative when $z = 1$ ($\chi = 0$), and positive when $z \to +\infty$ ($\chi \to +\infty$). To show that the sign changes exactly once, we differentiate the numerator in (D.4) and obtain the quadratic

$$6\alpha z^2 - 12\alpha z + 12\hat{\alpha}.$$

The discriminant of this quadratic, $144\alpha(\alpha - 2\hat{\alpha})$, is negative provided $\hat{\alpha} > 4\ \alpha/2$, a condition that clearly holds in our case since $\alpha \approx 40$ and $\hat{\alpha} \approx 1200$. Therefore, the numerator in (D.4) is an increasing function of $z$ and as such, it changes sign from negative to positive exactly once. We conclude that $\sigma(\chi)$ admits a unique minimum on the interval $[\chi_1; \chi_2]$ where it is positive.

## References


Abramson, J., Smirnova, I., Kasho, V., Verner, G., Kaback, H.R., Iwata, S., 2003. Structure and mechanism of the lactose permease of *Escherichia coli*. Science 301 (5633), 610–615.

Babloyantz, A., Sanglier, M., 1972. Chemical instabilities of all-or-none type in β-galactosidase induction and active transport. FEBS Lett. 23, 364–366.

Barkley, M.D., Riggs, A.D., Jobe, A., Burgeois, S., 1975. Interaction of effecting ligands with lac repressor and repressor–operator complex. Biochemistry 14 (8), 1700–1712.

Booth, I.R., Hamilton, W.A., 1980. Quantitative analysis of proton-linked transport system. β-galactoside exit in *Escherichia coli*. Biochem. J. 188 (2), 467–473.

Chung, J.D., Stephanopoulos, G., 1996. On physiological multiplicity and population heterogeneity of biological systems. Chem. Eng. Sci. 51, 1509–1521.

Cohen, G.N., Monod, J., 1957. Bacterial permeases. Bacteriol. Rev. 21 (3), 169–194.

Cohn, M., Horibata, K., 1959. Inhibition by glucose of the induced synthesis of the β-galactoside-enzyme system of *Escherichia coli*. Analysis of maintenance. J. Bacteriol. 78, 601–612.

Dekel, E., Alon, U., 2005. Optimality and evolutionary tuning of the expression level of a protein. Nature 436 (7050), 588–592.

Herzenberg, L.A., 1959. Studies on the induction of β-galactosidase in a cryptic strain of *Escherichia coli*. Biochim. Biophys. Acta 31 (2), 525–538.

Kepes, A., 1960. Kinetic studies on galactoside permease of *Escherichia coli*. Biochim. Biophys. Acta 40, 70–84.

Kepes, A., 1969. Carrier properties of β-galactoside permease. The role of the permease in the leak of *Escherichia coli*. In: Tosteson, D.C. (Ed.), Molecular Basis of Membrane Function. Prentice-Hall, Englewood Cliffs, NJ, pp. 353–389.

Kimata, K., Takahashi, H., Inada, T., Postma, P., Aiba, H., 1997. cAMP receptor protein-cAMP plays a crucial role in glucose-lactose diauxie by activating the major glucose transporter gene in *Escherichi coli*. Proc. Natl. Acad. Sci. USA 94, 12914–12919.

Koch, A.L., 1964. The role of the permease in transport. Biochim. Biophys. Acta 79, 177–200.

Kuhlman, T., Zhang, Z., Saier, M.H., Hwa, T., 2007. Combinatorial transcriptional control of the lactose operon of *Escherichia coli*. Proc. Natl. Acad. Sci. USA 104 (14), 6043–6048.

Lancaster, J.R., Hill, R.J., Struve, W.G., 1975. The characterization of energized and partially de-energized (respiration-independent) beta-galactoside transport into *Escherichia coli*. Biochim. Biophys. Acta 401 (2), 285–298.

Laurent, M., Kellershohn, N., 1999. Multistability: a major means of differentiation and evolution in biological systems. Trends Biochem. Sci. 24 (11), 418–422.

Laurent, M., Charvin, G., Guespin-Michel, J., 2005. Bistability and hysteresis in epigenetic regulation of the lactose operon. Since Delbrück, a long series of ignored models. Cell Mol. Biol. 51 (7), 583–594 (Noisy-le-grand).

Lewis, M., 2005. The lac repressor. C. R. Biol. 328 (6), 521–548.

Maloney, P.C., Wilson, T.H., 1973. Quantitative aspects of active transport by the lactose transport system of *Escherichia coli*. Biochim. Biophys. Acta 330 (2), 196–205.

McGinnis, J.F., Paigen, K., 1969. Catabolite inhibition: a general phenomenon in the control of carbohydrate utilization. J. Bacteriol. 100 (2), 902–913.

Mitchell, W.J., Misko, T.P., Roseman, S., 1982. Sugar transport by the bacterial phosphotransferase system. Regulation of other transport systems (lactose and melibiose). J. Biol. Chem. 257 (23), 14553–14564.

Narang, A., 2007. Effect of DNA looping on the induction kinetics of the lac operon. J. Theor. Biol. 247, 695–712.

Narang, A., Pilyugin, S.S., 2008. Bistability of the lac operon during growth of *Escherichia coli* on lactose and lactose + glucose. Bull. Math. Biol. 70 (4), 1032–1064.

Narang, A., Konopka, A., Ramkrishna, D., 1997. New patterns of mixed substrate growth in batch cultures of *Escherichia coli* K12. Biotech. Bioeng. 55, 747–757.

Novick, A., Weiner, M., 1957. Enzyme induction as an all-or-none phenomenon. Proc. Natl. Acad. Sci. USA 43, 553–566.

Oehler, S., Eismann, E.R., Krämer, H., Müller-Hill, B., 1990. The three operators of the lac operon cooperate in repression. EMBO J. 9 (4), 973–979.

Oehler, S., Amouyal, M., Kolkhof, P., von Wilcken-Bergmann, B., Müller-Hill, B., 1994. Quality and position of the three lac operators of *E. coli* define efficiency of repression. EMBO J. 13 (14), 3348–3355.

Oehler, S., Alberti, S., Müller-Hill, B., 2006. Induction of the lac promoter in the absence of DNA loops and the stoichiometry of induction. Nucleic Acids Res. 34 (2), 606–612.

Ozbudak, E.M., Thattai, M., Lim, H.N., Shraiman, B.I., van Oudenaarden, A., 2004. Multistability in the lactose utilization network of *Escherichia coli*. Nature 427, 737–740.

Saiz, L., Vilar, J.M.G., 2008. Ab initio thermodynamic modeling of distal multisite transcription regulation. Nucleic Acids Res. 36 (3), 726–731 ⟨http://dx.doi.org/10.1093/nar/gkm1034⟩.

Santillán, M., Mackey, M.C., Zeron, E.S., 2007. Origin of bistability in the lac operon. Biophys. J. 92 (11), 3830–3842.

Savageau, M.A., 2001. Design principles for elementary gene circuits: elements, methods, and examples. Chaos 11 (1), 142–159.

Segel, I.H., 1975. Enzyme Kinetics: Behavior and Analysis of Rapid Equilibrium and Steady-State Enzyme Systems. Wiley-Interscience, New York.

Tian, T., Burrage, K., 2005. A mathematical model for genetic regulation of the lactose operon. In: Gervasi, O., Gavrilova, M.L., Kumar, V., Lagana, A., Lee, H.P., Mun, Y., Taniar, D., Tan, C.J.K. (Eds.), Lecture Notes in Computer Science, vol. 3841. Springer, Berlin.

van Hoek, M.J.A., Hogeweg, P., 2006. In silico evolved lac operons exhibit bistability for artificial inducers, but not for lactose. Biophys. J. 91 (8), 2833–2843.

Vilar, J.M.G., Guet, C.C., Leibler, S., 2003. Modeling network dynamics: the lac operon, a case study. J. Cell. Biol. 161 (3), 471–476.

Winkler, H.H., Wilson, T.H., 1966. The role of energy coupling in the transport of β-galactosides by *Escherichia coli*. J. Biol. Chem. 241 (10), 2200–2211.

Yagil, G., Yagil, E., 1971. On the relation between effector concentration and the rate of induced enzyme synthesis. Biophys. J. 11, 11–27.